Inaugural-Dissertation

zur
Erlangung der Doktorwürde
der
Naturwissenschaftlich-Mathematischen Gesamtfakultät
der
Ruprecht-Karls-Universität
Heidelberg

vorgelegt von

Sara Lee

aus Seoul, Südkorea

Tag der mündlichen Prüfung:

Adaptive Multirate Method for Coupled Parabolic and Elliptic Equations

Gutachter: Dr. Thomas Carraro

Tag der mündlichen Prüfung:

Abstract

In this thesis, motivated by the simulation of fuel cells and batteries, we develop an adaptive discretization algorithm to reduce the computational cost for solving the coupled parabolic/elliptic system. This system is the model for the electrochemical processes within the cathode of a solid oxide fuel cell (SOFC). First, the coupled system is discretized in time and in space by the Finite Element Method. Then, it is split into parabolic and elliptic sub-problems through an operator splitting method. These two equations are solved sequentially by the multirate iterative solving method that allows for different time step sizes for the temporal discretizations.

The main focus of this work is to derive goal-oriented, a posteriori error estimators based on the Dual Weighted Residual method that are computable and separately assess the temporal discretization error, the spatial discretization error and the splitting error for each sub-problem. Instead of natural norms, the errors are measured in an arbitrary quantity of interest, as is often used in practical applications.

The sub-problems are solved in temporal discretizations with different step lengths. If the ratio between the two step lengths is too large, this can result in the divergence of the coupling iteration within the multirate scheme. In this case, the algorithm uses the information from the splitting error estimator to control the convergence behavior. The error contributions of both discretizations and splitting method are balanced at the end of the refinement cycle that halts when the error estimators reach a desired accuracy.

The described methods are validated on a simplified model that simulates the cathode of a SOFC. In this application, the parabolic part consists of a reaction-diffusion equation describing the concentration distribution of ions, and the elliptic part describes electrical potential. For a given accuracy, the adaptive algorithm finds the least required number of degrees of freedom of the parabolic and the elliptic parts of the system. Since the electrical potential equation has the faster time scale, we use the multirate method and see that the elliptic problem requires a smaller number of degrees of freedom to attain the same desired accuracy within the system. This significantly saves the total computational cost, since the elliptic equation in the coupled system is more expensive to solve. Therefore, this combination of the degrees of freedoms is optimal, in that it gives the least computational cost and the convergence within the algorithm.

Zusammenfassung

Gegenstand dieser Arbeit ist die Entwicklung eines adaptiven Diskretisierungsalgorithmus, der den Rechenaufwand zur Lösung des gekoppelten parabolisch/elliptischen Systems, das die elektrochemischen Prozesse in der Kathode einer Festoxidbrennstoffzelle (SOFC) beschreibt, reduziert. Zunächst wird das gekoppelte System in der Zeit und im Raum durch die Finite-Elemente-Methode diskretisiert. Dann wird es durch ein Operator-Splitting-Verfahren in ein parabolisches und ein elliptisches Problem aufgeteilt. Diese beiden Gleichungen werden abwechselnd durch eine iterative Multirate-Methode gelöst, die verschiedene Zeitschrittweiten für die zeitlichen Diskretisierungen erlaubt.

Der Schwerpunkt dieser Arbeit liegt in der Entwicklung von zielorientierten, a posteriori Fehlerschätzer auf der Basis der dual-gewichteten Residuenmethode und der Aufteilung der Schätzer in den zeitlichen und räumlichen Diskretisierungsfehler. Außerdem leiten wir auch einen Fehlerschätzer für das Splitting-Verfahren her. Durch diese berechenbaren Schätzer können wir den Fehler in Beiträge der zeitlichen und räumlichen Diskretisierungen jedes Teilproblems sowie der Splitting-Methode aufteilen. Anstatt natürliche Normen zu verwenden, werden die Fehler bezüglich beliebiger Fehlerfunktionale gemessen, die häufig in der Praxis eingesetzt werden.

Die Teilprobleme werden mit verschiedenen Zeitschrittweiten für die Zeitdiskretisierung gelöst. Falls das Verhältnis der Zeitschrittweiten zu groß ist, könnte das Multirate Schema divergieren. In diesem Fall verwendet der Algorithmus die Informationen aus dem Fehlerschätzer des Splitting-Verfahrens, um das Konvergenzverhalten zu steuern, indem die Zeitschrittweiten angepasst werden. Die Fehlerbeiträge von Diskretisierungs- und Splitting-Verfahren werden am Ende eines Verfeinerungszyklus ausgeglichen, der bis sie eine gewünschte Genauigkeit erreichen geht.

Die entwickelten Verfahren werden auf ein vereinfachtes Modell zur Simulation einer SOFC-Kathode angewendet. In dieser Anwendung besteht der parabolische Teil aus einer Reaktions-Diffusionsgleichung, die die Konzentrationsverteilung von Ionen beschreibt, während der elliptische Teil ein elektrisches Potential darstellt. Für eine gegebene Genauigkeit bestimmt der adaptive Algorithmus die kleinste erforderliche Anzahl der Freiheitsgrade für den parabolischen und elliptischen Teil des Systems. Da die elektrische Potentialgleichung die schnellere Zeitskala hat, verwenden wir die Multirate-Methode und sehen, dass das elliptische Problem eine geringere Anzahl von Freiheitsgrade benötigt um die gewünschte Genauigkeit innerhalb des Systems zu erreichen. Dies spart erheblich Rechenaufwand, da es teurer ist die elliptische Gleichung im gekoppelten System zu lösen. Diese Kombination der Freiheitsgrade ist die optimale in einem Sinne, dass es den geringsten Rechenaufwand und die Konvergenz innerhalb des Algorithmus gibt.

Contents

1 Introduction

The motivation behind this thesis as well as a brief discussion of the methods to approach the problem is presented in Section 1.1. An overview of the thesis can be found in Section 1.2.

1.1 Motivation and Goals

We briefly introduce fuel cells and describe how they work to generate electricity. Then, we elaborate on the goals of this thesis and methods used to achieve them.

1.1.1 Fuel cells

Fuel cells are electrochemical conversion devices that produce electricity and heat directly from fuel through a reaction with an oxidizing agent. In most types of fuel cells, the fuel contains hydrogen; through the electrochemical reaction of hydrogen and oxygen, electricity is generated when the oxygen ions release the electrons to combine with hydrogen molecules to form water.
The fuel cell consists of an electrolyte separating two electrodes: a cathode and an anode. At the cathode, the oxygen molecules from the air are split into oxygen ions. The oxygen ions are then transported through the electrolyte and combined with hydrogen at the anode, releasing two electrons per hydrogen molecule. The electrons travel an external circuit, providing electric power and producing heat as a by-product, as seen in Figure 1.1. The described chemical reactions can be expressed as follows:

$$\begin{aligned} \text{Anode Reaction} &: 2H_2 + 2O^{2-} \rightarrow 2H_2O + 4e^- \\ \text{Cathode Reaction} &: O_2 + 4e^- \rightarrow 2O^{2-} \end{aligned}$$

The fuel that can be used for fuel cells varies from pure hydrogen to natural gas, methanol and methane [46]. This variety increases a cell's flexibility because hydrogen is not naturally available in pure form. Yet, one must remain careful in choosing the fuel. For example, hydrocarbons, despite their availability and low production cost,

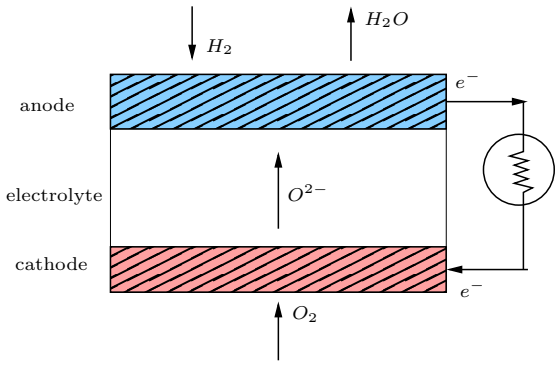

Figure 1.1. Schematic processes in an H_2 fuel cell. This thesis will focus on the cathode, one of the hindrances of the development of the SOFC technology.

produce carbon dioxide at the end of the process, which is one of the main causes of global warming [19, 20].

The fuel cells can be categorized based on the operating temperature of the electrolyte and fuel. The low temperature is in the range of $50 - 250\,^{\circ}\mathrm{C}$ for proton exchange membrane fuel cells (PEMFC), alkaline fuel cells (AFC) and phosphoric acid fuel cells (PAFC). The high operating temperature is in the range of $650 - 1000\,^{\circ}\mathrm{C}$ for molten carbonate fuel cells (MCFC) and solid oxide fuel cells (SOFCs).

In this thesis we consider SOFCs that are known to be the most useful devices for medium and large power applications due to their higher efficiency, as high as 75% [68]; internal reforming allows hydrogen to be extracted from the fuel, and waste heat can be recycled to make additional electricity by a cogeneration operation [32, 69]. Moreover, a SOFC can operate on many different fuels: hydrogen, methanol, ethanol, methane, propane, coal-derived syngas, or even diesel-reformats. In 2009, Chueh presented schemes to produce hydrogen from water using sunlight [17], which would make SOFCs the leading technology for producing electrical power directly from hydrogen.

Although fuel cells look promising as an efficient alternative source of clean energy, many hindrances remain. The main objection of SOFCs is the high cost of device construction. A fuel cell's layout influences its performance. For example, the economic way to structure fuel cells is in a stack. However, metal interconnections are not strong enough to maintain structural integrity at higher temperatures. Especially in cathodes, the metal stack's low reactivity and degradation in high temperature [68] exacerbates the problems.
Ongoing research has presented possible cathode materials that have excellent catalytic, electrochemical and mechanical properties. Yet, such materials (e.g. platinum)

can be very expensive [48]. Therefore, a stronger scientific understanding of the complex process of fuel cells is needed to discern ways of making the material more cost-efficient with the strongest layout [45].

Running a numerical simulation is a low-cost and flexible option for testing and development of new materials, fuels, and geometries. Moreover, it allows us to measure internal variables which are experimentally difficult or impossible to obtain in a real-world situation. It helps us to study the effects of various operating parameters on efficiency, current density and temperature, with more options and lower costs than experiments. The simulation of SOFCs involves a large number of parameters and a complicated structure system, primarily using Partial Differential Equations (PDEs). Therefore, a Finite Element method (FEM) is commonly used.

Due to the complexity of the model, we simplify the equations or fix the parameters as long as we maintain the acceptable range of accuracy in the result. Note that with regard to the development of fuel cells, the greater interest is not the distribution of the species, but rather their effect on the performance of the device.

1.1.2 Goals of the thesis

A simplified mathematical model of a cathode of a SOFC consists of the coupled parabolic and elliptic equations:

$$\alpha_1 \frac{\partial u(x,t)}{\partial t} - \alpha_2 \Delta u(x,t) - \alpha_3 \Delta v(x,t) = f, \tag{1.1a}$$

$$-\Delta v(x,t) + \alpha_4 v(x,t) - \alpha_5 u(x,t) = g, \tag{1.1b}$$

where u represents the oxygen ion concentration, v the electrical potential and f, g the external forces. The positive constant coefficients α_i represent the integer charge of the ion, its diffusivity, and its characteristic time and space scale. The detailed physical model and the derivation of the mathematical model are given in Chapter 2.

An operator splitting method is often used for problems that are hard to solve numerically when restrictions on accuracy can be relaxed because this method allows for an easier numerical treatment [39]. The idea behind the method is that it splits the model into a set of sub-equations so that it is possible to combine pre-developed numerical methods in a straightforward manner. In the case of an ill-conditioned coupled system, we can split the system into sub-parts so that each part will be well-conditioned. For the above system, the decoupling is done by splitting it into parabolic (1.1a) and elliptic (1.1b) equations. For example, the splitting method has been studied for coupled hyperbolic-parabolic systems in [30, 31, 39] and for coupled

multiphase flow and geomechanics in [3, 44]. This splitting method introduces an error called the *splitting error*.

For a numerical simulation of (1.1), we *discretize* the problems; in other words, we approximate the solution by a FEM. Taking into account that we have a non-stationary part in the system, we discretize in time, as well as in space. This discretization process carries along another source of the error, the *discretization error* in time and in space. The computational cost of numerically solving complex systems can be very high, especially for these non-stationary, coupled systems. Thus, it is important to develop an adaptive method to efficiently increase the accuracy of the approximation. For an efficient numerical adaptive scheme, we need to separate quantitative information about the discretization errors from the splitting error in order to gain the control over the error contributions from different sources.

Adaptive methods have been used in wide context (see Babuška and Strouboulis [8] and Verfürth [73]), but mostly in error estimates for natural norms. For example, Eriksson, Estep, Hansbo, and Johnson [26] developed an adaptive method based on a posteriori error estimates in the L^2-norm (see Bänsch [10], Grätsch and Bathe [36], and Houston, Schötzau, and Wihler [40] for more examples). However, in the case of fuel cells, the error estimation with respect to a natural norm is not very efficient. In most of the cases, we are interested in specific functional values of the solution, the so-called *quantity of interest*. For instance, this quantity can be the concentration of species at the boundary (the surface of the cathode) where the chemical reaction with the oxygen occurs, or it can be the concentration at the end of the reaction process.
Such estimation is developed by a *goal-oriented a posteriori error estimator* that is based on the *Dual Weighted Residual (DWR) Method* of Becker and Rannacher [11]. Schmich and Vexler [64] worked for (nonlinear) parabolic partial differential equations and separated the total discretization error into contributions due to the discretization in time and in space. This estimator gives information on the accuracy of the approximation and, moreover, provides a set of local error indicators that contains information to be used for a local mesh refinement for a possible future work.

In the context of parabolic problems, we refer to the works of Thomée [70], Meidner and Vexler [51, 52] and the sequential work of Eriksson, Johnson, and Larson [22–24, 27] on adaptive FEM for a linear parabolic problem and its error estimates, and additionally, the work of Eriksson and Johnson [25] on a nonlinear parabolic problem. Moreover, Akrivis, Makridakis, Ricardo, and Nochetto [2] derived a posteriori error estimates for time discretization by the Crank-Nicolson method. Space-time Galerkin methods have already been applied successfully to the simulation of incompressible flows (see, for examples, Cockburn, Karniadakis, and Shu [18], N'dri, Garon, and Fortin [57], and Mittal, Ratner, Hastreiter, and Tezduyar [54]). Nazarov and Hoffman

[56] [38] developed an adaptive algorithm for Navier-Stokes equations based on a posteriori error estimation. Van der Vegt and Van der Ven [72], more specifically, developed an algorithm for Euler equations. However, the temporal and spatial discretization errors were not separated. Instead, the temporal refinement was linked to the spatial refinement.

The present work extends the derivation of the discretization error by separating into the temporal and spatial discretization errors for the coupled linear problems with the additional factor of time dependency. We derive a posteriori error estimators that are separated into the temporal and spatial discretization errors, and then further parceled into the splitting error for each sub-problem. The development of the adaptive mesh refinement algorithm uses the error estimators to decide which discretization to refine in order to reduce the computational cost.

To date, the author knows of no work done on a posteriori error estimation of the splitting method for non-stationary problems. However, for the stationary problems, the control of these errors has been developed for various linear problems, such as: the simple Poisson equation; the Stokes equations in fluid mechanics; and the KKT system of linear-quadratic elliptic optimal control problems by Meidner, Rannacher, and Vihharev [50]; a second-order elliptic model problem by Jiránek, Strakoš, and Vohralík [42]; and linear elliptic problems by Arioli, Liesen, Miçdlar, and Strakoš [4] and Rannacher, Westenberger, and Wollner [62]. Moreover, for nonlinear elliptic problems the error contribution (referred as the *iteration error*) is developed by Ern and Vohralík [29] and Rannacher and Vihharev [60].

The additional unique quality of this work is the development of an efficient discretization refining technique for the coupled parabolic/elliptic system solved by a multirate iterative solving method. Since the diffusion equation of ions and the electric potential equation have different characteristic time scales, it is natural to consider a multirate scheme. The scheme exploits the different time step sizes for the parabolic and elliptic equations. The development and analysis of theoretically convergent iterative coupling algorithms have been studied in the recent works of Almani, Dogru, Kumar, Singh, and Wheeler [3], Kim, Tchelepi, and Juanes [43] and Mikelic and Wheeler [53]. If the ratio between the total number of time steps between the equations is too large, the algorithm diverges.

Localized error indicators obtained by the DWR method allow the set up of a versatile algorithm for adaptive mesh refinement and the equilibration of temporal and spatial discretization errors with the splitting error. The discretizations are independently refined until the corresponding error estimators reach a given tolerance. Particularly, the derived splitting error estimate is used to ensure the convergence of the algorithm.

1.2 Overview

In **Chapter 2**, the mathematical model of a fuel cell cathode is introduced. We discuss under which assumptions the model has been derived and simplified. Also the boundary conditions are presented.

In **Chapter 3**, we set the notation used throughout the thesis.

In **Chapter 4**, we develop the temporal and spatial discretizations by Galerkin methods. The spatial discretization is done by a continuous Galerkin scheme, cG($\cdot$). For the temporal discretization, we use two time schemes: dG(0), the variant of the implicit Euler method and cG(1), the variant of the Crank-Nicolson method. To deal with the instabilities due to inexact initial values, we apply the damped Crank-Nicolson time stepping scheme as proposed in the work of Luskin, Rannacher, and Wendland [47].

The multirate iterative method is presented in detail in **Chapter 5**. The system is split into two sub-parts: parabolic and elliptic equations; these are solved on different time scales. The discrete equations are stated for the multirate scheme, and the coupling iteration is performed in order to increase the accuracy of solutions. A complication of working with different time scales will be addressed: approximated coupling terms.

In **Chapter 6**, the performance in the quantity of interest is evaluated by the a posteriori error estimation based on the Dual Weighted Residual (DWR) method, using the solutions of dual problems. Then, the estimates separately assess the error due to the discretization in time and space of each sub-problem. Additionally, we explain how using the splitting method causes the Galerkin perturbation and derive the error estimate of the perturbation method. By using these estimates, we develop an adaptive algorithm for the combination of temporal and spatial discretizations with the least computational cost while ensuring the convergence of the coupling iteration within the splitting method.

In **Chapter 7**, we apply the developed adaptive refinement technique and present numerical results. The error estimates are validated by comparing them with the error functionals.

The thesis is concluded in **Chapter 8**, where we summarize and discuss the possible extensions of this research in the future.

2 Modeling a Fuel Cell Cathode

In this chapter, we first present the equations describing the electrochemical process in the cathode. Then, under a few assumptions and linearization, we obtain the simplified mathematical model and its boundary conditions that we consider in this thesis. The simplified model can be found in Section 2.4.

2.1 Basic Equations

A set of three fundamental equations governs charge transport in solids: transport equation, continuity equation and total charge in the electric potential system. The first fundamental equation is the generalized transport equation that relates the driving force (electrochemical potential) to the mass flux

$$\mathbf{J}_i^{mass}(x,t) = -\frac{\sigma_i(x,t)}{(z_i e)^2}\frac{\partial \tilde{\mu}_i(x,t)}{\partial x}, \tag{2.1}$$

where x is position and t is time and i is the species of charge carrier, $i = eon, ion$. Also z_i is the integer charge of species, e is the elementary charge of an electron, $\mathbf{J}_i^{mass}(x,t)$ is the carrier mass flux, $\tilde{\mu}_i(x,t)$ is the electrochemical potential and $\sigma_i(x,t)$ is the electrical conductivity defined by

$$\sigma_i(x,t) = \frac{D_i(z_i e)^2}{k_B T} c_i(x,t) \tag{2.2}$$

by the Nernst-Einstein relation. We assume that the diffusivity D_i are independent of position and concentration. $c_i(x,t)$ is the carrier concentration, k_B is the Boltzmann constant and T is the absolute temperature.
The reduced electrochemical potential $\tilde{\mu}_i^*(x,t)$ is

$$\begin{aligned}\tilde{\mu}_i^*(x,t) &= \frac{\tilde{\mu}_i(x,t)}{z_i e} \\ &= (\tilde{\mu}_i^*)^o + \frac{k_B T}{z_i e}\ln\left(\frac{c_i(x,t)}{c_i^o}\right) + \phi(x,t),\end{aligned}$$

where ϕ is the electric potential. Then, its derivative is

$$\frac{\partial \tilde{\mu}_i^*(x,t)}{\partial x} = \frac{k_B T}{z_i\, e} \frac{\nabla c_i(x,t)}{c_i(x,t)} + \nabla\phi(x,t). \tag{2.3}$$

With the carrier charge flux

$$\mathbf{J}_i^{charge}(x,t) = z_i\, e\, \mathbf{J}_i^{mass}(x,t), \tag{2.4}$$

we write (2.1) in terms of charge flux and reduced potential:

$$\mathbf{J}_i^{charge}(x,t) = -\sigma_i(x,t) \frac{\partial \tilde{\mu}_i^*(x,t)}{\partial x}. \tag{2.5}$$

The second fundamental equation describes the continuity. In the case where there are no internal sources or sinks of mass, its continuity requires that the variation in mass flux with respect to position balances with the variation in concentration with respect to time, i.e., in terms of the charge flux:

$$z_i e \frac{\partial c_i(x,t)}{\partial t} + \frac{\partial}{\partial x} \mathbf{J}_i^{charge}(x,t) = 0.$$

The last fundamental equation relates the sum of the charges in the system to the electric potential:

$$-\epsilon_o \epsilon_r \Delta\phi(x,t) = e \sum_i z_i c_i(x,t)\,,$$

where ϵ_o is the vacuum permittivity and ϵ_r is the relative permittivity.

2.2 Approximation

Assume that σ_{eon} is large and $\mathbf{J}_{eon}^{charge}$ is sufficiently small from (2.5), which hold true for the cathode materials with the good electrical conductivity. Then, $\tilde{\mu}_{eon}^*$ becomes constant and the approximation is

1. $\tilde{\mu}_{eon}^*$ is constant, (2.6)
2. $\partial_t c_{ion}(x,t) + \nabla(-\sigma_{ion}(x,t)\, \nabla \tilde{\mu}_{ion}^*(x,t)) = 0,$ (2.7)
3. $-\epsilon_o \epsilon_r \Delta\phi = e(z_{ion} c_{ion}(x,t) + z_{eon} c_{eon}(x,t)).$ (2.8)

2.2.1 Dimensionless

To transform into the dimensionless form, we apply the transformations $(x,t) \to (\tilde{x},\tilde{t})$ such that $x = l_c\,\tilde{x}$ and $t = \tau\,\tilde{t}$ for some scaling factors l_c, τ. This implies that

$$\nabla_x(\cdot) = \frac{1}{l_c}\nabla_{\tilde{x}}(\cdot) \quad \text{and} \quad \partial_t(\cdot) = \frac{1}{\tau}\,\partial_{\tilde{t}}\,(\cdot)\,.$$

Next, define new parameters in the table below.

V_{th}	k_BT/e
$\widetilde{\phi}$	ϕ/V_{th}
τ_{eon}	$l_c^2/\bar{D}_{eon}$
τ_{ion}	$l_c^2/\bar{D}_{ion}$
τ	$\min(\tau_{ion},\tau_{eon})$
$\widetilde{c}_i$	$c_i/\bar{c}_i$
$\widetilde{D_i}$	$D_i/\bar{D}_i$

First, recall Equation (2.3). Then, for constant $\tilde{\mu}^*_{eon}$ (2.6), we can say that a small perturbation $\delta\tilde{\mu}^*_{eon}$ is zero, i.e.,

$$\frac{V_{th}}{z_{eon}}\frac{\delta c_{eon}(x,t)}{\bar{c}_{eon}} + \delta\phi = 0.$$

In the dimensionless form, it is written as

$$\delta c_{eon} = -z_{eon}\delta\phi. \tag{2.9}$$

Secondly, substitute (2.2) and (2.3) into (2.7) for $i = ion$ and obtain

$$z_{ion}e\,\partial_t c_{ion} = \nabla\cdot\left[\frac{D_{ion}(z_{ion}e)^2}{k_BT}c_{ion}(x,t)\left(\frac{V_{th}}{z_{ion}c_{ion}}\frac{\nabla c_{ion}(x,t)}{c_{ion}(x,t)} + \nabla\phi\right)\right].$$

Simplifying it further, we obtain

$$\partial_t c_{ion} = D_{ion}\Delta c_{ion}(x,t) + \frac{D_{ion}z_{ion}}{V_{th}}\nabla(c_{ion}(x,t)\nabla\phi(x,t)),$$

whose dimensionless form is

$$\frac{\tau_{ion}}{\tau}\partial_{\tilde{t}}\tilde{c}_{ion} = \tilde{D}_{ion}\nabla_{\tilde{x}}\cdot\left(\nabla_{\tilde{x}}\tilde{c}_{ion}(x,t) + z_{ion}\tilde{c}_{ion}(x,t)\nabla_{\tilde{x}}\tilde{\phi}\right). \tag{2.10}$$

Lastly, the dimensionless form of (2.8) is

$$\Delta_{\tilde{x}}\tilde{\phi} = -\frac{l_c^2}{\epsilon_o\epsilon_r}\frac{e}{V_{th}}(z_{ion}\bar{c}_{ion}\tilde{c}_{ion} + z_{eon}\bar{c}_{eon}\tilde{c}_{eon}). \tag{2.11}$$

2.2.2 Linearization

Consider the situation upon application of a small perturbation such as a sinusoidal signal, a square-wave signal or other periodic or aperiodic form. For a sufficiently small perturbation, it is possible to write the quantities as the sum of their steady state values and the time-dependent perturbations:

$$\tilde{c}(x,t) = \bar{c}(x) + \delta c(x,t), \tag{2.12a}$$

$$\tilde{\phi}(x,t) = \bar{\phi}(x) + \delta\phi(x,t). \tag{2.12b}$$

Substitute (2.12) into (2.10) and we obtain:

$$\frac{\tau_{ion}}{\tau}\partial_{\tilde{t}}\delta c_{ion}(x,t) = \tilde{D}_{ion}\nabla_{\tilde{x}}\cdot\left(\nabla_{\tilde{x}}\delta c_{ion} + z_{ion}\nabla_{\tilde{x}}\delta\phi\right). \tag{2.13}$$

Also linearize (2.11) with Debye length $\lambda_D^2 = \epsilon_o\epsilon_r V_{th}/e$:

$$\Delta_{\tilde{x}}\delta\phi = -\left(\frac{l_c}{\lambda_D}\right)^2\left(z_{ion}\bar{c}_{ion}\delta c_{ion} + z_{eon}\bar{c}_{eon}\delta c_{eon}\right).$$

We perform the Fourier transformation on (2.13) after the substitution of (2.9), and we obtain the equations in terms of δc_{ion} and $\delta\phi$:

$$\frac{\tau_{ion}}{\tau}\delta c_{ion}(x,t) = \tilde{D}_{ion}\Delta_{\tilde{x}}\delta c_{ion} + z_{ion}\bar{c}_{ion}\tilde{D}_{ion}\bar{c}_{ion}\Delta_{\tilde{x}}\delta\phi \tag{2.14a}$$

$$\Delta_{\tilde{x}}\delta\phi = -\left(\frac{l_c}{\lambda_D}\right)^2\left(z_{ion}\bar{c}_{ion}\delta c_{ion} - z_{eon}^2\bar{c}_{eon}\delta\phi\right). \tag{2.14b}$$

2.3 Boundary Conditions

The boundary conditions are as follows after linearizing in dimensionless form.
For Γ_1,

$$\delta c_{ion} = 0,$$
$$\delta\phi = 0.$$

For Γ_2 and Γ_3,

$$\partial_{\mathbf{n}}\delta c_{ion} = 0,$$
$$\partial_{\mathbf{n}}\delta\phi = 0.$$

For Γ_4,

$$\partial_{\mathbf{n}}\delta c_{ion} = -\partial_{\mathbf{n}}\phi,$$
$$\delta\phi = 1.$$

Lastly, for Γ_5,

$$\begin{aligned} \partial_{\mathbf{n}}\delta c_{ion} &= -\delta c_{ion}, \\ \partial_{\mathbf{n}}\delta\phi &= -\delta c_{ion}. \end{aligned}$$

Figure 2.1 shows how the boundaries are divided on $\partial\Omega$. Setting both sides of the cathode, Γ_2, Γ_3, with the homogeneous Neumann boundary condition, indicates the relative-thin structure of the cathode. Moreover, the dotted line in the figure indicates e.g., a metal collector. Thus, the upper boundaries Γ_4 and Γ_5 have different boundary conditions. The triple phase boundary (TPB) is indicated where gas phase, oxide and metal meet and electrochemical conversion occurs.

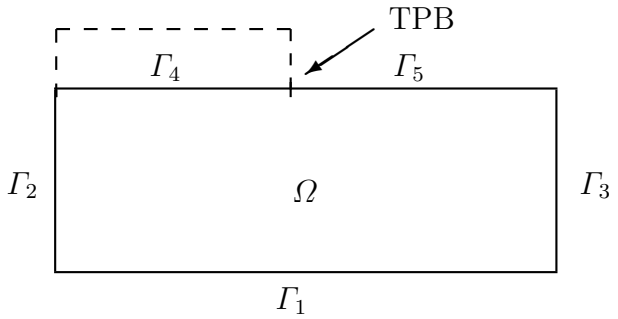

Figure 2.1. Sketch of the boundaries as indicated.

2.4 Simplified Mathematical Model

We divide (2.14a) by $\frac{\tau_{ion}}{\tau}$ and write the coefficient in (2.14) as α_i, $i = 1, \cdots, 5$ and denote $u := \delta_{\tilde{t}} c_{ion}$ and $v := \delta\phi$:

$$\begin{aligned} \alpha_1 \frac{\partial u(x,t)}{\partial t} - \alpha_2 \Delta u(x,t) - \alpha_3 \Delta v(x,t) &= f, \\ -\Delta v(x,t) + \alpha_4 v(x,t) - \alpha_5 u(x,t) &= g, \end{aligned}$$

where $\alpha_1 = 1$ is omitted to write from this point on.

Remark 2.1. Note that the functions on the right-hand side f, g are zero in this derivation. In our calculations, however, we choose an arbitrary f, g to calculate the exact solutions to use them to test the solution behaviors such as their convergence rate.

3 Notations and Variational Formulation

Throughout this thesis, let Ω be a bounded domain with the boundary denoted as $\partial\Omega$. In general, we can assume the boundary to be the Lipschitz boundary. For an introduction into Sobolev space, we refer to standard text books, e.g. Adams and Fourier [1], Grisvard[37] or Wloka[75] where a precise definition of the Lipschitz boundary is presented.

For a variational formulation, introduce the Hilbert spaces $V := H_0^1(\Omega)$ and $H := L^2(\Omega)$. Let V^* denote the topological dual of V, then $V \hookrightarrow H \hookrightarrow V^*$ constitutes a Gelfand triple. For all $t \in I := (0,T)$, we define the biliear form $\bar{a}_1 : (V\times V)\times V \to \mathbb{R}$ and $\bar{a}_2 : (V \times V) \times V \to \mathbb{R}$ by

$$\begin{aligned}\bar{a}_1(u(t),v(t))(\phi(t)) &:= \alpha_2(\nabla u(t),\phi(t)) + \alpha_3(\nabla v(t),\phi(t)),\\ \bar{a}_2(u(t),v(t))(\psi(t)) &:= (\nabla v(t),\nabla\psi(t)) + \alpha_4(v(t),\psi(t)) - \alpha_5(u(t),\psi(t)),\end{aligned}$$

where $u(t)$ and $v(t)$ live in the function space

$$X(0,T) := \left\{x(t) \in L^2(I,V) \text{ and } \partial_t x \in L^2(I,V^*); t \in I\right\}.$$

This space X is embedded in the respective space of continuous functions, i.e., $X \hookrightarrow C(\bar{I},V)$ [55, 75]. Moreover, the operators $a_1 : (X \times X) \times X \to \mathbb{R}$ and $a_2 : (X \times X) \times X \to \mathbb{R}$ are the integrations of $\bar{a}_1$ and $\bar{a}_2$ over time:

$$\begin{aligned}a_1(u,v)(\phi) &:= \int_I \bar{a}_1(u(t),v(t))(\phi(t))\,dt,\\ a_2(u,v)(\psi) &:= \int_I \bar{a}_2(u(t),v(t))(\psi(t))\,dt,\end{aligned}$$

for $\phi(t)$ and $\psi(t) \in X$. With the simplified notations:

$$\begin{aligned}((u(t),v(t))) &:= \int_\Omega\int_I u(t)\,v(t)\,dt\,dx,\\ (u(t),v(t)) &:= (u(t),v(t))_H,\end{aligned}$$

write the system (1.1) for all $t > 0$ in the following weak formulation for a solution $u(t), v(t) \in X$:

$$\begin{aligned}
((\partial_t u(t), \phi(t))) + a_1(u(t), v(t))(\phi(t)) &= (f(t), \phi(t)) \quad \forall \phi(t) \in X, && \text{(3.1a)}\\
(u(0), \phi(0)) &= (u_0, \phi(0)),\\
a_2(u(t), v(t))(\psi(t)) &= (g(t), \psi(t)) \quad \forall \psi(t) \in X, && \text{(3.1b)}\\
(v(0), \psi(0)) &= (v_0, \psi(0)),
\end{aligned}$$

where $f, g \in L^2(I, V^*)$ and $u_0, v_0 \in H$ is the initial values. Note that initial value v_0 must satisfy Equation (3.1b):

$$a_2(u(0), v_0)(\psi(t)) = (g(t), \psi(t)) \quad \forall \psi(t) \in X\,.$$

Moreover, we define

$$\begin{aligned}
\mathcal{A}(u, v)(\varphi, \psi) &= (f(t), \phi(t)) - ((\partial_t u(t), \phi(t))) - a_1(u(t), v(t))(\phi(t)) && \text{(3.2)}\\
&\quad + (g(t), \psi(t)) - a_2(u(t), v(t))(\psi(t))\,.
\end{aligned}$$

4 Discretization

In this chapter, we describe the space-time finite element discretization of the weak formulation of the system (3.1). Here, we present the semi-discrete problem in time. The time discretization is offered as two types of discretization: discontinuous Galerkin dG and continuous Galerkin cG; and the space discretization is based on usual H^1-conforming finite elements.

4.1 Discretization in Time

The first type of the time discretization used in this thesis is the *discontinuous Galerkin method of degree r* or simply $dG(r)$ method. This method uses discontinuous trial and test functions, which are piecewise polynomials of degree r. The second method is the *continuous Galerkin method of degree r* or $cG(r)$ method. This method uses continuous trial functions of piecewise polynomials of degree r and the discontinuous test functions. In cases where the method uses the test and trial functions from different function spaces, we specify it as *Petrov-Galerkin method*.
For the semi-discretization in time, we partition the time interval $\bar{I} = [0, T]$ into

$$\bar{I} = \{0\} \cup I_1 \cup \cdots \cup I_M,$$

where subintervals $I_m := (t_{m-1}, t_m]$ of length $k_m := t_m - t_{m-1}$ with given time points

$$0 = t_0 < \cdots < t_m < \cdots < t_M = T.$$

The discretization parameter k_m is given as a piecewise constant function by setting $k\,|_{I_m} := k_m$ for $m = 1, \ldots, M$. On the subintervals I_m, we define the following semi-discrete space X_k^r, which we use for a trial space in the continuous Galerkin method for $r \in \mathbb{N}$ as

$$X_k^r := \left\{ x_k \in C(\bar{I}, H) \,\middle|\, x_k|_{I_m} \in P_r(\bar{I}_m, V),\, m = 1, \ldots, M \right\}.$$

where $H = L^2(\Omega)$ and $V = H_0^1(\Omega)$. $P_r(I_m, V)$ denotes the space of polynomials up to degree r on I_m with values in V. Moreover, let us define another semi-discrete

space $\widetilde{X}_k^r$ used for the trial and test space in the discontinuous Galerkin method and the test space in the continuous Galerkin method as

$$\widetilde{X}_k^r := \left\{ x_k \in L^2(I,V) \,\middle|\, x_k|_{I_m} \in P_r(I_m,V) \text{ and } x_k(0) \in H,\, m = 1,\dots,M \right\}.$$

To account for the possible discontinuity of a function $x_k \in \widetilde{X}_k^r$ at time point t_m, we introduce the standard notations for the limits from the right x_k^{m+}, the limits from the left x_k^{m-} and the jumps $[x_k]_m$ of x at time point t_m:

$$x_k^{m\pm} := \lim_{\epsilon \to 0} x_k(t_m \pm \epsilon), \qquad [x_k]_m := x_k^{m+} - x_k^{m-}. \tag{4.1}$$

Discontinuous Galerkin methods

The dG(r) semi-discretization of the system reads:
Find $u_k, v_k \in \widetilde{X}_k^r$ satisfying

$$\begin{aligned} \sum_{m=1}^{M} \int_{I_m} (\partial_t u_k, \varphi) dt + a_1(u_k, v_k)(\varphi) + \sum_{m=0}^{M-1} ([u_k]_m, \varphi^+) + (u_k(0)^-, \varphi(0)^-) & \\ = \int_I (f,\varphi) + (u_0, \varphi(0)^-), & \\ a_2(u_k, v_k)(\psi) = \int_I (g,\psi), & \end{aligned}$$

$\forall u, v, \varphi, \psi \in \widetilde{X}_k^r$.

Remark 4.1. Note that the initial value for the second component v_0 does not appear for dG because the value $v(t_0 = 0)$ is not needed to calculate $v(t_1)$.

Continuous Galerkin methods

The cG(r) formulation with the semi-discrete spaces reads:
Find $u_k, v_k \in X_k^r$ satisfying

$$\begin{aligned} \int_I (\partial_t u_k, \varphi) dt + a_1(u_k, v_k)(\varphi) + (u_{k,0}, \varphi(0)^-) &= \int_I (f,\varphi)\, dt + (u_0, \varphi(0)^-), \\ a_2(u_k, v_k)(\psi) &= \int_I (g,\psi)\, dt, \\ (u_k(0)^-, \varphi(0)^-) &= (u_0, \varphi(0)^-), \\ (v_k(0)^-, \psi(0)^-) &= (v_0, \psi(0)^-), \end{aligned}$$

$\forall u, v \in X_k^r$ and $\forall \varphi, \psi \in \widetilde{X}_k^r$. As explained in the last chapter, v_0 is not chosen arbitrarily. It should satisfy that

$$a_2(u_k(0), v_0)(\psi) = \int_I (g, \psi)\, dt,$$

Remark 4.2. Due to the discontinuity of the test functions, the dG(0) decouples into a time-stepping scheme. Thus, the dG(0) discretization is a variant of the implicit (backward) Euler scheme. And cG(1) is a variant of the Crank-Nicolson scheme.

4.2 Discretization in Space

In this section, we describe the discretization in space of the semi-discrete problem in time derived in the previous section. So far we have considered the function spaces X_k^r and $\widetilde{X}_k^r$. These spaces contain the continuous spatial space $V := H_0^1$. Now we derive the fully discrete problems for the cG(s)dG(r) and cG(s)cG(r) discretizations. Following the notations defined in [28], cG(s)dG(r) denotes a space-time finite element discretization with continuous piecewise polynomials of degree s in space and discontinuous piecewise polynomials of degree r in time. Consequently, cG(s)cG(r) denotes a space-time finite element discretization with continuous piecewise polynomials of degree s in space and continuous piecewise polynomials of degree r in time.

The computation domain Ω consists of line, quadrilateral or hexahedral cells K for $d = 1, 2$ or 3, respectively. For the sake of simplicity, let us for the moment assume that the boundary $\partial\Omega$ is polygon. The cells K conform a non-overlapping cover of Ω forming the mesh denoted as T_h. The discretization parameter h is a cell-wise constant function that can be defined as $h\,|_K := h_K$, where h_K is the diameter of the cell $K \in T_h$. Following the descriptions in Bangerth and Rannacher [9], Braess [14], Brenner and Scott [15], we formulate the definition of regularity:

Definition 4.1. *A mesh T_h is called* regular *if the following conditions are satisfied:*

i. $\bar{\Omega} = \cup_{k \in T_h} \bar{K}$.

ii. $K \cap K' = \emptyset$ *for all cells* $K, K' \in T_h$ *with* $K \neq K'$.

iii. *Any face of any K is either a subset of the boundary $\partial\Omega$ or a face of another cell.*

The condition (iii) can be relaxed to allow hanging nodes (shown in Figure 4.1) for case of using a local mesh refinement and also to allow non-polygonal boundary $\partial\Omega$

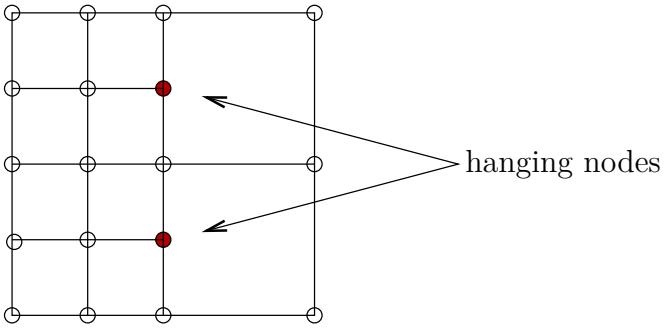

Figure 4.1. Two dimensional meshes with hanging nodes as indicated.

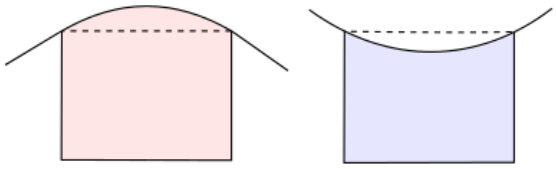

Figure 4.2. Examples of the domain with non-polygonal boundary.

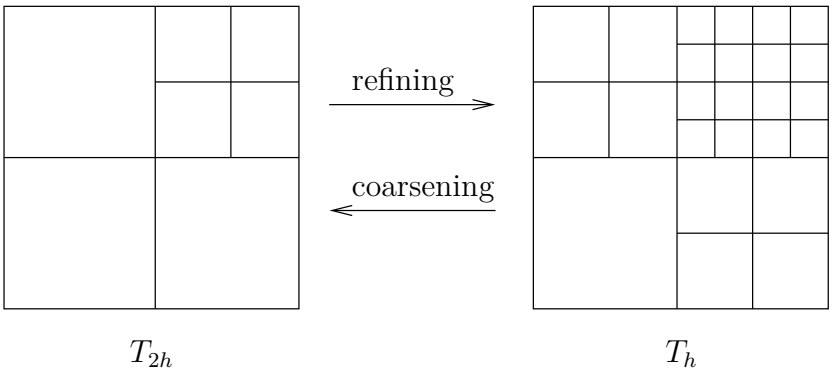

Figure 4.3. Two-dimensional mesh T_{2h} and corresponding finer mesh T_h produced in a patch-wise manner.

(see Figure 4.2). Note that hanging nodes do not carry any degrees of freedom, and usually only up to one hanging node per each cell is allowed.

The mesh refinement is executed in a patch-wise manner, i.e., the next mesh T_h is obtained by the refining, uniformly or adaptively, of a coarser mesh T_{2h}, e.g. Figure 4.3.

Another important condition on the geometry of the cell is the uniformity which is defined as: there is κ such that $\frac{h}{\rho_K} \leq \kappa$ for all $K \in T_h$, where ρ_K is the radius of the biggest inscribed circle of K [14]. In plain terms, it does not allow any cells that are too long, narrow or pointy. Each refined mesh must meet this condition in order to ensure approximation properties of the finite element spaces.
On the mesh T_h, a conforming finite element space $V_h^s \subset V$ is defined as

$$V_h^s := \{v \in V \mid v|_K \in Q_s(K) \quad \text{for } K \in T_h\}$$

where $Q_s(K)$ is obtained by using the inverse transformations $\sigma^{-1} : K \to \hat{K}$ by

$$Q_s(K) := \left\{v_h : K \to \mathbb{R} \mid v_h(\sigma(\cdot)) \in \hat{Q}_s(\hat{K})\right\}$$

where $\hat{Q}_s(\hat{K})$ is the space of tensor product polynomials up to degree s on the reference cell $\hat{K} = (0,1)^d$. The lowest order $s = 1$ results in the space of bi-linear functions ($d = 2$)

$$\hat{Q}_s(\hat{K}) = \text{span}\,\{1, \hat{x}_1, \hat{x}_2, \hat{x}_1\hat{x}_2\}.$$

Although the concepts for the hanging nodes, mesh uniformity and its refinement and boundary conditions are explained in this section for possible extension to the cases for $d = 2, 3$, in this thesis, calculations are done for $d = 1$, so the concepts are greatly simplified.

4.3 Formulation with Time-Stepping Schemes

In this section, we explicitly present the formulation of our system as time-stepping schemes of the space-time Galerkin finite element discretization. Now let us define the fully discrete space-time finite element spaces that we will use in the rest of the thesis:

$$X_{kh}^{r,s} := \left\{x_{kh} \in C(\bar{I}, H) \,\middle|\, x_{kh}|_{I_m} \in V_h^s,\ m = 1, \ldots, M\right\} \tag{4.3}$$

$$\widetilde{X}_{kh}^{r,s} := \left\{x_{kh} \in L^2(I, V) \,\middle|\, x_{kh}|_{I_m} \in P_r(I_m, V_h^s),\ x_{kh}(0) \in V_h^s,\ m = 1, \ldots, M\right\} \tag{4.4}$$

Note that we have $X_{kh}^{r,s} \subset X_k^r$ and $\widetilde{X}_{kh}^{r,s} \subset \widetilde{X}_k^r$.
In the following sections, we use the notations

$$u_{kh}^0 = u_{kh}(0) \in V_h^s \quad \text{and} \quad u_{kh}^m = u_{kh}(t_m) \in V_h^s, \quad v_{kh}^m = v_{kh}(t_m) \in V_h^s,$$

for $m = 1, \cdots, M$.

4.3.1 cG(s)dG(0) discretization

Consider the case of the cG(s)dG(0) discretization.

and obtain the following discrete equations:
For $m = 0$,

$$(u_{kh}^0, \varphi) \;=\; (u_0, \varphi) \quad \forall \varphi \in V_h^s,$$

and for $m = 1, \cdots, M$,

$$\begin{aligned} (u_{kh}^m, \varphi) + k_m \bar{a}_1(u_{kh}^m, v_{kh}^m)(\varphi) &= (u_{kh}^{m-1}, \varphi) + \int_{I_m} (f(t), \varphi)\, dt \quad \forall \varphi \in V_h^s, \\ \bar{a}_2(u_{kh}^m, v_{kh}^m)(\psi) &= \int_{I_m} (g(t), \psi)\, dt \quad \forall \psi \in V_h^s. \end{aligned}$$

The temporal integral is approximated by using the box rule:

$$\int_{I_m} (f(t), \varphi)\, dt \approx k_m (f(t_m), \varphi) =: k_m (f^m, \varphi)$$

and the formulation is written explicitly as

$$(u_{kh}^m - u_{kh}^{m-1}, \varphi) + \alpha_2 k_m (\nabla u_{kh}^m, \nabla \varphi) + \alpha_3 k_m (\nabla v_{kh}^m, \nabla \varphi) = k_m (f^m, \varphi) \quad (4.5a)$$

$$(\nabla v_{kh}^m, \nabla \psi) + \alpha_4 (v_{kh}^m, \psi) - \alpha_5 (u_{kh}^m, \psi) = (g^m, \psi) \quad (4.5b)$$

$\forall \varphi, \psi \in V_h^s$ and for $1 = 1, \cdots, M$.

Remark 4.3. We take the test functions $\varphi, \psi \in \widetilde{X}_{kh}^{0,1}$, i.e., piecewise constant over the time interval. Then, by taking the end time value on I_m, we can choose test functions independent of time. Therefore, use $\varphi, \psi \in V_h^s$ for the cG(s)dG(0) scheme as above. This applies in the same way for the cG(s)cG(1) scheme.

Remark 4.4. Based on how we have defined the time interval I_m, we approximate the time integrals by the box rule; this is then equivalent to the implicit Euler method, which is known to be of first order and strongly A-stable [16].

4.3.2 cG(s)cG(1) discretization

For $m = 0$,

$$(u_{kh}^0, \varphi) \;=\; (u_0, \varphi) \quad \forall \varphi \in V_h^s,$$

and for $m = 1, \cdots, M$,

$$(u_{kh}^m, \varphi) + \int_{I_m} \bar{a}_1 \left(\frac{1}{k_m} (t - t_{m-1})\, u_{kh}^m - (t - t_m)\, u_{kh}^{m-1} \right) (\varphi)\, dt$$
$$= (u_{kh}^{m-1}, \varphi) + \int_{I_m} (f(t), \varphi)\, dt \quad \forall \varphi \in V_h^s,$$

$$\int_{I_m} \bar{a}_2 \left(\frac{1}{k_m} (t - t_{m-1})\, v_{kh}^m - (t - t_m)\, v_{kh}^{m-1} \right) (\varphi) dt = \int_{I_m} (g(t), \psi)\, dt \quad \forall \psi \in V_h^s.$$

The time integrals can be approximated by the trapezoidal rule or by the Gaussian quadrature rule. Using the trapezoidal rule, we obtain the usual Crank-Nicolson method:
For $m = 0$,

$$(u_{kh}^0, \varphi) \;=\; (u_0, \varphi) \quad \forall \varphi \in V_h^s,$$

and for $m = 1, \cdots, M$,

$$(u_{kh}^m, \varphi) + \frac{1}{2} k_m \bar{a}_1 (u_{kh}^m, v_{kh}^m)(\varphi)$$
$$= (u_{kh}^{m-1}, \varphi) - \frac{1}{2} k_m \bar{a}_1 (u_{kh}^{m-1}, v_{kh}^{m-1})(\varphi) + \int_{I_m} (f(t), \varphi)\, dt \quad \forall \varphi, \in V_h^s,$$
$$\frac{1}{2} k_m \bar{a}_2 (u_{kh}^m, v_{kh}^m)(\psi) = -\frac{1}{2} k_m \bar{a}_2 (u_{kh}^{m-1}, v_{kh}^{m-1})(\psi) + \int_{I_m} (g(t), \psi)\, dt \quad \forall \psi, \in V_h^s.$$

And the explicit formulations are

$$(u_{kh}^m, \varphi) + \frac{k_m}{2} \Big[\alpha_2 (\nabla u_{kh}^m, \nabla \varphi) + \alpha_3 (\nabla v_{kh}^m, \nabla \varphi) \Big]$$
$$= (u_{kh}^{m-1}, \varphi) + \frac{k_m}{2} (f^m + f^{m-1}, \varphi) + \frac{k_m}{2} \Big[\alpha_2 \left(\nabla u_{kh}^{m-1}, \nabla \varphi \right) + \alpha_3 \left(\nabla v_{kh}^{m-1}, \nabla \varphi \right) \Big],$$

$$\Big[(\nabla v_{kh}^m, \nabla \psi) + \alpha_4 (v_{kh}^m, \psi) - \alpha_5 (u_{kh}^m, \psi) \Big]$$
$$= (g^m + g^{m-1}, \varphi) + \Big[\left(\nabla v_{kh}^{m-1}, \nabla \psi \right) + \alpha_4 \left(v_{kh}^{m-1}, \psi \right) - \alpha_5 \left(u_{kh}^{m-1}, \psi \right) \Big].$$

for all $\varphi, \psi \in V_h^s$.

Remark 4.5. The Crank-Nicolson scheme is known to be of second order and only A-stable, not strongly A-stable.

4.4 The Damped Crank-Nicolson Scheme

In certain cases using the multirate solving method that will be introduced in Chapter 5, we observe the divergence of the adaptive algorithm we aim to develop. Although the Crank-Nicolson scheme gives second-order convergence, it is not guaranteed to achive convergence, due to possible irregularities of initial conditions. Thus, we introduce the damped Crank-Nicolson scheme, which is the Crank-Nicolson method with a certain amount of damping, as proposed by Luskin, Rannacher, and Wendland [47][61]. They proved that the number of damping steps needed depends on the lack of regularity in the initial conditions.
We can ensure the convergence by replacing one or more steps of the Crank-Nicolson method with that of the implicit Euler scheme. Applying this idea for the time-stepping scheme, we restate the time intervals for the damped Crank-Nicolson scheme.

Choose the number of damping steps L, $0 \leq L \leq M$ such that it ensures the convergence under the given initial conditions. Let J_L be the corresponding set of indices, $J_L = \{\ell_1, \ldots, \ell_L\} \subset 1, \ldots, M$. For $\ell \in J_L$, the interval is split into two equal intervals: define $t_{\ell-1/2} := t_\ell - \frac{1}{2}k_\ell$ for $k_l = |l|$. Now define the interval J^0 where steps by the implicit Euler method are applied and J^1 for the Crank-Nicolson method by

$$\begin{aligned} J^0 &= \{\ell, \ell - \frac{1}{2} \mid \ell \in J_L\} \quad \text{and} \quad J^1 = J \setminus J^0 \\ \text{where} \quad J &= J^0 \cup \{n \in \mathbb{N} \mid 1 \leq \mathrm{n} \leq \mathrm{M}\}. \end{aligned}$$

Then we can redefine the intervals I_m as

$$I_m = \begin{cases} (t_{m-1}, t_m], & m \in J^1, \\ (t_{m-\frac{1}{2}}, t_m], & m \in J^0. \end{cases}$$

Therefore, the damped Crank-Nicolson method is as follows:
Given u_o, for $m = 0$,

$$(u^0_{kh}, \varphi) = (u_0, \varphi) \quad \forall \varphi \in L^2(\Omega),$$

for $m \in J^0$,

$$\begin{aligned} (u^m_{kh}, \varphi) + k_m \bar{a}_1(u^m_{kh}, v^m_{kh})(\varphi) &= (u^{m-\frac{1}{2}}, \varphi) + \int_{I_m} (f(t), \varphi)\, dt \quad \forall \varphi \in V^s_h, \\ \bar{a}_2(u^m_{kh}, v^m_{kh})(\psi) &= \int_{I_m} (g(t), \psi)\, dt \quad \forall \psi \in V^s_h, \end{aligned}$$

and for $m \in J^1$,

$$(u_{kh}^m, \varphi) + \frac{1}{2} k_m \bar{a}_1(u_{kh}^m, v_{kh}^m)(\varphi)$$
$$= (u_{kh}^{m-1}, \varphi) - \frac{1}{2} k_m \bar{a}_1(u_{kh}^{m-1}, v_{kh}^{m-1})(\varphi) + \int_{I_m} (f(t), \varphi)\, dt \qquad \forall \varphi \in V_h^s,$$
$$\frac{1}{2} k_m \bar{a}_2(u_{kh}^m, v_{kh}^m)(\psi) = -\frac{1}{2} k_m \bar{a}_2(u_{kh}^{m-1}, v_{kh}^{m-1})(\psi) + \int_{I_m} (g(t), \psi)\, dt \qquad \forall \psi \in V_h^s.$$

5 Splitting Method and Multirate Iterative Coupling Scheme

We consider an operator splitting method for the coupled parabolic/elliptic system. The method decouples the system by splitting it into two sub-parts: parabolic and elliptic equations. We adapt the multirate iterative coupling scheme that employs the different time step length for the equations as follows: take multiple finer time steps for the parabolic equation within one coarser time step of the elliptic equation. We present a fully discrete scheme using the implicit Euler time discretization scheme.

5.1 Operator Splitting Method

Due to the high computational cost of solving complex coupled systems, various coupling methods have been developed and applied, for example, to describe the interactions between flow and geomechanis (Fredrich, Arguello, Deitrick, De Rouffignac, et al. [33], Jha and Juanes [41], Tran, et al. [71], Zhai and Chen [76], and Dean, et al. [21]). Coupling methods are typically classified into three types: fully (implicit) coupling, iterative (sequential), and loosely (weak) coupled methods.

The fully coupled approach solves the two coupled equations simultaneously and obtains so-called "simultaneous solutions". These solutions are unconditionally stable and make the method robust. However, the method is, in general, computationally expensive and might create other computational difficulties for the linear solvers for coupled systems.

The iterative (sequential) method solves, for example in this system, the parabolic, or the elliptic, problem first, and then the other problem is solved using the intermediate solution information. The stability and the convergence of the sequential method for a coupled geomechanical and reservoir model have been studied by Prevost [59], Settari and Walters [65], Wheeler and Gai [74], and Sattari, et al. [66]. The sequential procedure is iterated at each time step until an adequate degree of accuracy is obtained. Ideally, the solutions converge to the simultaneous solutions at the end of this coupling iteration. For its advantages, instead of requiring to develop solvers designed for given coupled systems, the iterative approach has the freedom to use

standard solvers. The iterative method has also been used as a pre-conditioner for the fully coupled method. In their works, Gai, et al. [34] applied it as a pre-conditioning to a Richardson fixed point iteration.

Lastly, the loosely coupled method is a special case of the sequential method with one iteration. The computational cost is least of the three, but solutions can be inexact and only conditionally stable (refer the work of Armero and Simo [5], [6]). By decoupling the system, the latter two methods need less computational storage space. However, compared to the fully coupling method that guarantees the same-order convergence with the order of the chosen time scheme, the convergence of the sequential method depends on the splitting strategy [43].

The operator splitting of the coupled parabolic/elliptic system for the implicit Euler time scheme is as follows:

$$\begin{aligned}(u_{kh}^m - u_{kh}^{m-1}, \varphi) + \alpha_2 k_m(\nabla u_{kh}^m, \nabla\varphi) + \alpha_3 k_m(\nabla v_{kh}^m, \nabla\varphi) &= k_m(f^m, \varphi) \qquad \forall\varphi \in \widetilde{X}_{kh}^{0,1},\\ (\nabla v_{kh}^m, \nabla\psi) + \alpha_4(v_{kh}^m, \psi) - \alpha_5(u_{kh}^m, \psi) &= (g^m, \psi) \qquad \forall\psi \in \widetilde{X}_{kh}^{0,1}.\end{aligned}$$

The system can be also written in the matrix form,

$$\begin{aligned}(M_u + \alpha_2 k_m A_u)\, u_{kh}^m + \alpha_3 k_m A_{uv} v_{kh}^m &= M_u u_{kh}^{m-1} + k_m\, f_m,\\ (A_v + \alpha_4 M_v)\, v_{kh}^m - \alpha_5 M_{uv} u_{kh}^m &= g_m,\end{aligned}$$

where $f_m := (f^m, \varphi)$ and $g_m := (g^m, \psi)$, and the matrices are defined as

$$\begin{aligned}(M_u)_{ji} &= (\varphi_i^m, \varphi_j^m), & (M_v)_{ji} &= (\psi_i^m, \psi_j^m),\\ (A_u)_{ji} &= (\nabla\varphi_i^m, \nabla\varphi_j^m), & (A_v)_{ji} &= (\nabla\psi_i^m, \nabla\psi_j^m),\\ (A_{uv})_{ji} &= (\nabla\psi_i^m, \nabla\varphi_j^m) & (M_{uv})_{ji} &= (\psi_i^m, \varphi_j^m)\end{aligned}$$

.

For the h-refinement, the condition number of the stiffness matrix A is estimated by $O(h^{-2})$, and the condition number of the mass matrix M is uniformly bounded, $O(1)$ [7, 15]. Thus, the most expensive part of the computational cost is to invert the stiffness matrix. However, since the diffusion equation is time dependent, we consider the matrix $(M_u + \alpha_2 k_m A_u)$ whose condition number is $O(k_m\, h^{-2})$. Then, its condition number decreases as the time discretization is refined. For example, if $O(k_m) \approx O(h)$, the condition number of the diffusion equation decreases to $O(h^{-1})$. Therefore, with regard to saving on the computational cost, we must find a way to save the cost from the electric potential equation. One of the methods is to solve the potential equation until it is just good enough for the entire system not to diverge, rather than waiting until it converges to the simultaneous solution. This idea is explained later in more detail via diagrams and the algorithm.

5.2 Discrete Multirate Iterative Scheme

As the diffusion equation of ions and the electric potential equation have different characteristic time scales, it is natural to consider the multirate scheme. Since the electric potential equation has the faster time scale [63], we expect to see that the discretization for the elliptic equation remains coarser than for the parabolic equation.
Here, we provide a multirate formulation for the sequential coupling method introduced in the previous section. We choose different temporal discretizations for the parabolic and elliptic equations. We use the simplified notation for the fully discretized system in space and time:

$$u^n := u^n_{kh} \quad \text{and} \quad v^n := v^n_{kh}.$$

Suppose the parabolic problem is solved on the finer time mesh with total M time steps and the elliptic equation on the coarser time mesh with M/q time steps. Thus, within one coarser time step, there are q finer corresponding local time steps for each sequential coupling iteration. By using the finite element method in space and the implicit Euler method in time, the weak formulation of a multirate scheme reads as follows:
Find $u^{m+n} \in \widetilde{X}^{0,1}_{kh}$ for $1 \le n \le q$ satisfying

$$\left(\frac{u^{m+n} - u^{m+n-1}}{k_{m+n}}, \varphi\right) + \alpha_2(\nabla u^{m+n}, \nabla\varphi) + \alpha_3(\nabla v^{\widetilde{m}+1}, \nabla\varphi) = (f^{m+n}, \varphi) \quad (5.1a)$$

and find $v_i^{\widetilde{m}+1} \in \widetilde{X}^{0,1}_{kh}$ satisfying

$$(\nabla v^{\widetilde{m}+1}, \nabla\psi) + \alpha_4(v^{\widetilde{m}+1}, \psi) - \alpha_5(\bar{u}^m, \psi) = (g^{\widetilde{m}+1}, \psi) \quad (5.1b)$$

for $\varphi, \psi \in \widetilde{X}^{0,1}_{kh}$. The set $\widetilde{X}^{0,1}_{kh}$ is as defined in (4.4).
The time index m increases as the multiple of q:

$$m = 1, q, 2q, \cdots, M. \quad (5.2)$$

The time index for v on the coarser temporal discretization is denoted as $\widetilde{m} := \frac{m}{q}$, and the average value over the local time steps as

$$\bar{u}^m := \frac{1}{q}\sum_{n=1}^{q} u^{m+n}. \quad (5.3)$$

The results, on each iteration, obtain q intermediate solutions u^{m+n} $(n = 1, \cdots, q)$ of the parabolic equation and one intermediate solution $v^{\widetilde{m}+1}$ for the elliptic equation. This process is iterated within one coarser time step until the solutions are obtained with an acceptable tolerance.

As an example, in a case where the parabolic equation (5.1a) is solved first, the coupling value $v^{\widetilde{m}+1}$ is not available. We can use a general guessing value denoted as $\widetilde{v}^{\widetilde{m}+1}$, and this leads to inexact solutions $\widetilde{u}^{m+n}$ for $n = 1, \cdots, q$. Consequently, the solution of (5.1b) will be also inexact. Using these inexact intermediate solutions as coupling values introduces the *splitting error*.
Here, we provide a multirate iterative coupling scheme for the fully discrete multirate scheme in (5.1). Within a coarser time step $\widetilde{m}$, we perform the coupling (fixed point) iteration whose index is denoted as i. For the unknown coupling value $v_i^{\widetilde{m}+1}$ at the i-th iteration, we make an educated guess; we use the value from the previous iteration for v:

$$v_i^{\widetilde{m}+1} = v_{i-1}^{\widetilde{m}+1}.$$

In case of $i = 0$, use the value from the previous time step:

$$v_0^{\widetilde{m}+1} = v^{\widetilde{m}}.$$

Then, Equation (5.1) at i-th iteration is written as:

$$\left(\frac{u_i^{m+n} - u_i^{m+n-1}}{k_{m+n}}, \varphi\right) + \alpha_2(\nabla u_i^{m+n}, \nabla\varphi) + \alpha_3(\nabla v_{i-1}^{\widetilde{m}+1}, \nabla\varphi) = (f^{m+n}, \varphi), \quad (5.6a)$$

$$(\nabla v_i^{\widetilde{m}+1}, \nabla\psi) + \alpha_4(v_i^{\widetilde{m}+1}, \psi) - \alpha_5(\bar{u}_i^m, \psi) = (g^{\widetilde{m}+1}, \psi) \quad (5.6b)$$

$\forall\varphi, \psi \in \widetilde{X}_{kh}^{0,1}$. Note that in (5.6a), we take the coupling value v_{i-1} from the previous iteration since it is solved first. On the other hand, in Equation (5.6b), we use the coupling values $\bar{u}_i$ at the i-th iteration. With a number of iterations, we expect the intermediate solutions to converge to the simultaneous solutions, i.e., $u_i^m \to u^m$ and $v_i^m \to v^m$ as $i \to \infty$. See the diagram below to understand the iterative process within one coarser time step.

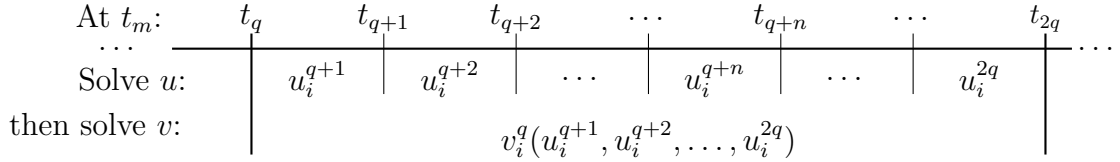

Figure 5.1. Two different time discretizations. There are q finer time steps for each coarser time step.

Notation clarification are as follows: i denotes the coupling iteration index, which shows the number of iterations on a coarser time step until convergence or until it

reaches the maximum number of iterations; m is the finer time step index; q is a fixed number of finer time steps per coarser time step; n is the local time step index for finer mesh on each coarser time step, $1 \leq n \leq q$.

Remark 5.1. We anticipate that the error depends on the parameter q, which is the same as the ratio between the total number of time steps of two meshes. We observe in a later chapter that there are some restrictions on the ratio and, thus, we develop an adaptive refinement algorithm that provides a way to search for an optimal ratio to solve the system accurately and efficiently.

5.3 Algorithms

In this section, we present three algorithms to compare the fully coupled (non iterative) method, the single rate iterative method, and the multirate iterative method for the fully discretized system. The first algorithm shows the fully implicit approach, where both components are solved simultaneously with no multirate method applied.

Algorithm 1 Fully Implicit Algorithm

1: **procedure** GIVEN u^0, SOLVE v^0.
2: **for** $m = 1, 2, \ldots, M$ **do**
3: solve the fully discretized u^m and v^m satisfying for all $\varphi, \psi \in \widetilde{X}_{kh}^{0,1}$:

$$\begin{aligned} \left(\frac{u^m - u^{m-1}}{k_m}, \varphi\right) + \alpha_2 \left(\nabla u^m, \nabla \varphi\right) + \alpha_3 \left(\nabla v^m, \nabla \varphi\right) &= \left(f^m, \varphi\right) \\ \left(\nabla v^m, \nabla \psi\right) + \alpha_4 \left(v^m, \psi\right) - \alpha_5 \left(u^m, \psi\right) &= \left(g^m, \psi\right) \end{aligned}$$

4: **end for**
5: **end procedure**

The second algorithm is for the single rate iterative method. Here, the system is decoupled and solved sequentially. The coupling terms are fed into the other equation as a force term. Since it is the single rate method, both components are solved on a same time discretization. The iteration continues until the intermediate solution u_i^m converges to the simultaneous solution u^mi.e.,

$$|u_i^m - u^m| < TOL \tag{5.7}$$

for a given tolerance TOL.

Algorithm 2 Single Rate Iterative Coupling Algorithm

procedure GIVEN u^0, SOLVE v^0.
  for $m = 1, 2, \ldots, M$ **do**
    for $i = 1, 2, \ldots$ **do**
      if $i = 1$ **then**
        set $v_{i-1}^m = v^{m-1}$
      end if
      Solve for the fully discretized $u_i^m(v_{i-1}^m)$ satisfying for all $\varphi, \psi \in \widetilde{X}_{kh}^{0,1}$:

$$\left(\frac{u_i^m - u^{m-1}}{k_m}, \varphi\right) + \alpha_2 \left(\nabla u_i^m, \nabla \varphi\right) \;=\; (f^m, \varphi) - \alpha_3 \left(\nabla v_{i-1}^m, \nabla \varphi\right)$$

      Given u_i^m, solve for v_i^m satisfying:

$$(\nabla v_i^m, \nabla \psi) + \alpha_4 \left(v_i^m, \psi\right) \;=\; (g^m, \psi) + \alpha_5 \left(u_i^m, \psi\right)$$

      if $|u_i^m - u^m < TOL|$ **then**
        end the loop i
      end if
    end for
  end for
end procedure

Lastly, we present the algorithm for the multirate iterative scheme for the coupled system.

Algorithm 3 Multirate Iterative Coupling Algorithm

procedure GIVEN u^0, SOLVE v^0.
  for $m = 0, q, 2q, \ldots, M$ **do**
    for $i = 1, 2, \ldots$ **do**
      if $i = 1$ **then**
        set $v_{i-1}^{\widetilde{m}+1} = v^{\widetilde{m}}$
      end if
      for $n = 1, 2, \ldots, q$ **do**
        Solve for the fully discretized $u_i^{m+n}(v_{i-1}^{\widetilde{m}+1})$ satisfying for all $\varphi, \psi \in \widetilde{X}_{kh}^{0,1}$:

$$\left(\frac{u_i^{m+n} - u_i^{m+n-1}}{k_{m+n}}, \varphi\right) + \alpha_2 \left(\nabla u_i^{m+n}, \nabla\varphi\right) \;=\; (f^{m+n}, \varphi) - \alpha_3 \left(\nabla v_{i-1}^{\widetilde{m}+1}, \nabla\varphi\right)$$

      end for
      Given $u_i^{m+1}, u_i^{m+2}, \ldots, u_i^{m+q}$, solve for $v_i^{\widetilde{m}+1}$ satisfying:

$$\left(\nabla v_i^{\widetilde{m}+1}, \nabla\psi\right) + \alpha_4 \left(v_i^{\widetilde{m}+1}, \psi\right) \;=\; \left(g^{\widetilde{m}+1}, \psi\right) + \alpha_5 \left(\bar{u}^m, \psi\right)$$

    end for
    if $|u_i^m - u^m < TOL|$ **then**
      end the loop i
    end if
  end for
end procedure

6 A Posteriori Error Estimation

In an adaptive finite element method, a posteriori error estimation in natural norms, such as the energy norm or the L_2 norm, is used for mesh refinement in order to equilibrate the local error indicators. However, the natural norms cannot provide information on local quantities. Thus, the error in the approximation of a quantity of interest is estimated in terms of local residuals of the computed solution, which is multiplied by weight factors. In the DWR method, these weights are the corresponding dual solutions.
In this thesis, the error estimator is separated into contributions from the discretization in time and in space for each sub-part of the system. In addition, the splitting error estimator is derived and balanced with the discretization errors within the refinement cycle. To the best of our knowledge, this is the first analysis of a posteriori error estimation for the splitting error by the multirate iterative solving method.

In this chapter, we derive the residuals using the DWR method for the coupled system. In Section 6.4, we present the explicit form of the localized residuals. In Section 6.5, we introduce the Galerkin perturbation and derive its error estimator. Lastly and most importantly, in Section 6.6, we present the main achievement of this thesis, the adaptive refinement algorithm.

6.1 Derivation of the A Posteriori Error Estimator

Recall the following result for the general situation of the Galerkin approximation of stationary points of functionals (Bangerth and Rannacher [9]).

Proposition 6.1. *Let $L(\cdot)$ be a three-times differentiable functional defined on a (real or complex) vector space Y which has a stationary point $x \in Y$, i.e.,*

$$L^{'}(x)(y) = 0 \quad \forall y \in Y. \tag{6.1}$$

Suppose that on a finite dimensional subspace $Y_h \subset Y$, the corresponding Galerkin approximation has a discrete solution $x_h \in Y_h$ satisfying

$$L^{'}(x_h)(y_h) = 0 \quad \forall y_h \in Y_h. \tag{6.2}$$

Then, the error representation for arbitrary $y_h \in Y_h$ is

$$L(x) - L(x_h) = \frac{1}{2} L^{'}(x_h)(x - y_h) + \mathcal{R}_h, \tag{6.3}$$

where the remainder $\mathcal{R}_h$ is cubic in the error $e := x - x_h$,

$$\mathcal{R}_h := \frac{1}{2} \int_0^1 L^{'''}(x_h + se)(e, e, e)s(s-1)ds.$$

Its proof can be found in [9].

Based on a posteriori error estimation by Schmich and Vexler [64] and Becker, Kapp, and Rannacher [12], we derive a posteriori error estimates that measure the discretization errors in a functional $J(\cdot)$ and separate the total discretization error into contributions due to temporal and spatial discretization of each sub-part such as

$$\begin{aligned} J(u,v) - J(u_{kh}, v_{kh}) &= (J(u,v) - J(u_k, v_k)) + (J(u_k, v_k) - J(u_{kh}, v_{kh})) \\ &\approx (\eta_k^u + \eta_k^v) + (\eta_h^u + \eta_h^v) \\ &=: \eta_k^{u+v} + \eta_h^{u+v}. \end{aligned} \tag{6.4}$$

In this coupled system, in addition to the refinement process keeping the temporal discretization error η_k^{u+v} and spatial discretization error η_h^{u+v} balanced, we also want to consider the balance between the sub-parts within a discretization: the balance between η_k^u and η_k^v and the balance between η_h^u and η_h^v. This enables more computational saving, as we will show in the later section.
In this thesis, we choose the error functional $J(\cdot)$ to be a continuous linear functional in form of

$$J(u,v) := \int_I J_1(u(t), v(t))\, dt + J_2(u(T), v(T)),$$

where $J_1 : V \to \mathbb{R}$ or $J_2 : H \to \mathbb{R}$ may be zero.

Define the product spaces:

$$\bar{X} := (X \times X) \times (X \times X), \tag{6.5a}$$
$$\bar{X}_k^r := (\widetilde{X}_k^r \times \widetilde{X}_k^r) \times (\widetilde{X}_k^r \times \widetilde{X}_k^r), \tag{6.5b}$$
$$\bar{X}_{kh}^{r,s} := (\widetilde{X}_{kh}^{r,s} \times \widetilde{X}_{kh}^{r,s}) \times (\widetilde{X}_{kh}^{r,s} \times \widetilde{X}_{kh}^{r,s}). \tag{6.5c}$$

We introduce the Lagrangian functional of the given system $\mathcal{L} : \bar{X} \to \mathbb{R}$, defined by

$$\begin{aligned} \mathcal{L}(u,v;z_1,z_2) &:= J(u,v) + (f - \partial_t u, z_1) - \alpha_2(\nabla u, \nabla z_1) - \alpha_3(\nabla v, \nabla z_1) \\ &\quad + (g, z_2) - (\nabla v, \nabla z_2) - \alpha_4(v, z_2) + \alpha_5(u, z_2) \\ &\quad - (u(0) - u_0, z_1(0)) \\ &=: J(u,v) - A_1(u,v)(z_1) - A_2(u,v)(z_2), \end{aligned} \tag{6.6}$$

where

$$\begin{aligned} A_1(u,v)(z_1) &= (\partial_t u, z_1) + \alpha_2(\nabla u, \nabla z_1) + \alpha_3(\nabla v, \nabla z_1) - (f, z_1) \\ &\quad +(u(0) - u_0, z_1(0)), \\ A_2(u,v)(z_2) &= (\nabla v, \nabla z_2) + \alpha_4(v, z_2) - \alpha_5(u, z_2) - (g, z_2). \end{aligned}$$

$u, v, u_k, v_k, u_{kh}, v_{kh}$ are called "primal variables" and $z_1, z_2, z_{1,k}, z_{2,k}, z_{1,kh}, z_{2,kh}$ "dual variables".

The time-discrete Lagrangian functional for the case of dG(r) discretization $\widetilde{\mathcal{L}} : \bar{X}_k^r \to \mathbb{R}$ is defined by

$$\begin{aligned} \widetilde{\mathcal{L}}(u_k, v_k; z_{1,k}, z_{2,k}) &:= J(u_k, v_k) + (f, z_{1,k}) - \sum_{m=1}^{M} \int_{I_m} (\partial_t u_k, z_{1.k})\, dt - \alpha_2(\nabla u_k, \nabla z_{1,k}) \\ &\quad -\alpha_3(\nabla v_k, \nabla z_{1,k}) - \sum_{m=0}^{M-1} ([u_k]_m, z_{1,k}^{m,+}) \\ &\quad +(g, z_{2,k}) - (\nabla v_k, \nabla z_{2,k}) - \alpha_4(v_k, z_{2,k}) + \alpha_5(u_k, z_{2,k}) \\ &\quad -(u_k(0) - u_0, z_{1,k}(0)), \end{aligned}$$

and for the case of cG(r) discretization $\widetilde{\mathcal{L}} : \bar{X}_k^r \to \mathbb{R}$ as

$$\begin{aligned} \widetilde{\mathcal{L}}(u_k, v_k; z_{1,k}, z_{2,k}) &:= J(u_k) + (f, z_{1,k}) - \sum_{m=1}^{M} \int_{I_m} (\partial_t u_k, z_{1,k})\, dt - \alpha_2(\nabla u_k, \nabla z_{1,k}) \\ &\quad - \alpha_3(\nabla v_k, \nabla z_{1,k}) + (g, z_{2,k}) - (\nabla v_k, \nabla z_{2,k}) - \alpha_4(v_k, z_{2,k}) \\ &\quad + \alpha_5(u_k, z_{2,k}) - (u_k(0) - u_0, z_1(0)). \end{aligned}$$

Let $(u, v; z_1, z_2) \in \bar{X}$, $(u_k, v_k; z_{1,k}, z_{2,k}) \in \bar{X}_k^r$, and $(u_{kh}, v_{kh}; z_{1,kh}, z_{2,kh}) \in \bar{X}_{kh}^{r,s}$ be stationary points of $\mathcal{L}$ and $\widetilde{\mathcal{L}}$, respectively, i.e.,

$$\mathcal{L}'(u, v; z_1, z_2)(\varphi, \psi; \chi, \xi) = 0 \quad \forall (\varphi, \psi; \chi, \xi) \in \bar{X}, \tag{6.7a}$$

$$\widetilde{\mathcal{L}}'(u_k, v_k; z_{1,k}, z_{2,k})(\varphi_k, \psi_k; \chi_k, \xi_k) = 0 \quad \forall (\varphi_k, \psi_k; \chi_k, \xi_k) \in \bar{X}_k^r, \tag{6.7b}$$

$$\widetilde{\mathcal{L}}'(u_{kh}, v_{kh}; z_{1,kh}, z_{2,kh})(\varphi_{kh}, \psi_{kh}; \chi_{kh}, \xi_{kh}) = 0 \quad \forall (\varphi_{kh}, \psi_{kh}; \chi_{kh}, \xi_{kh}) \in \bar{X}_{kh}^{r,s}. \tag{6.7c}$$

The case of the continuous problem (6.7a) implies that the primal solutions u, v are determined by the variational equations

$$\begin{aligned} \mathcal{L}'_{z_1}(u, v; z_1, z_2)(\chi) &= -A_1(u, v)(\chi) = 0 \quad \forall \chi \in X, \\ \mathcal{L}'_{z_2}(u, v; z_1, z_2)(\xi) &= -A_2(u, v)(\xi) = 0 \quad \forall \xi \in X, \end{aligned}$$

which involve the directional derivatives of the Lagrangian with respect to the dual variables. Correspondingly, the dual solutions z_1, z_2 are determined by

$$\mathcal{L}_u'(u,v;z_1,z_2)(\varphi) = J_u'(u,v)(\varphi) - A_{1,u}'(u,v)(\varphi,z_1) - A_{2,u}'(u,v)(\varphi,z_2) = 0 \quad \forall \varphi \in X,$$
$$\mathcal{L}_v'(u,v;z_1,z_2)(\psi) = J_v'(u,v)(\psi) - A_{1,v}'(u,v)(\psi,z_1) - A_{2,v}'(u,v)(\psi,z_2) = 0 \quad \forall \psi \in X,$$

which, this time, involve the directional derivatives of the Lagrangian, with respect to the primal variables. Similarly, the stationary points $u_k, v_k, z_{1,k}, z_{2,k} \in \widetilde{X}_k^r$ and $u_{kh}, v_{kh}, z_{1,kh}, z_{2,kh} \in \widetilde{X}_{kh}^{r,s}$ are solutions of the derivative of the semi-discrete in time (6.7b) and fully discrete Lagrangian (6.7c), respectively (not shown here). Then for arbitrary $(z_1, z_2) \in X \times X$, $(z_{1,k}, z_{2,k}) \in \widetilde{X}_k^r \times \widetilde{X}_k^r$, and $(z_{1,kh}, z_{2,kh}) \in \widetilde{X}_{kh}^{r,s} \times \widetilde{X}_{kh}^{r,s}$,

$$\begin{aligned} J(u,v) - J(u_k,v_k) &= \mathcal{L}(u,v;z_1,z_2) - \widetilde{\mathcal{L}}(u_k,v_k;z_{1,k},z_{2,k}) \\ &= \widetilde{\mathcal{L}}(u,v;z_1,z_2) - \widetilde{\mathcal{L}}(u_k,v_k;z_{1,k},z_{2,k}), \qquad (6.8) \\ J(u_k,v_k) - J(u_{kh},v_{kh}) &= \widetilde{\mathcal{L}}(u_k,v_k;z_{1,k},z_{2,k}) - \widetilde{\mathcal{L}}(u_{kh},v_{kh};z_{1,kh},z_{2,kh}). \qquad (6.9) \end{aligned}$$

It holds that $\mathcal{L}(u,v;z_1,z_2) = \widetilde{\mathcal{L}}(u,v;z_1,z_2)$ since the jump terms in $\widetilde{\mathcal{L}}$ vanish because the solutions are continuous in time. Now note that $\widetilde{X}_k^r \not\subset X$. Thus, in order to apply Proposition 6.1, we define the continuous space Y and the product spaces $\bar{Y}$ and $\bar{Y}_k$ as:
Let

$$\begin{aligned} \bar{Y} &:= (Y \times Y) \times (Y \times Y) \quad \text{for} \quad Y := (X \cup \widetilde{X}_k^r), \qquad (6.10a) \\ \bar{Y}_k &:= (\widetilde{X}_k^r \times \widetilde{X}_k^r) \times (\widetilde{X}_k^r \times \widetilde{X}_k^r), \qquad (6.10b) \end{aligned}$$

for Equation (6.8).
Since $\widetilde{X}_k^r \subset \widetilde{X}_{kh}^{r,s}$, for Equation (6.9), let

$$\begin{aligned} \bar{Y} &:= (\widetilde{X}_k^r \times \widetilde{X}_k^r) \times (\widetilde{X}_k^r \times \widetilde{X}_k^r), \\ \bar{Y}_k &:= (\widetilde{X}_{kh}^{r,s} \times \widetilde{X}_{kh}^{r,s}) \times (\widetilde{X}_{kh}^{r,s} \times \widetilde{X}_{kh}^{r,s}). \end{aligned}$$

Then, by Proposition 6.1, we have the following error representation:

$$J(u,v) - J(u_k,v_k) = \frac{1}{2}\widetilde{\mathcal{L}}'(u_k,v_k;z_{1,k},z_{2,k})(e_k^u, e_k^v; e_k^{z_1}, e_k^{z_2}) + \mathcal{R}_k \qquad (6.11)$$
$$J(u_k,v_k) - J(u_{kh},v_{kh}) = \frac{1}{2}\widetilde{\mathcal{L}}'(u_{kh},v_{kh};z_{1,kh},z_{2,kh})(e_{kh}^u, e_{kh}^v; e_{kh}^{z_1}, e_{kh}^{z_2}) + \mathcal{R}_h \qquad (6.12)$$

where $\mathcal{R}_k$ and $\mathcal{R}_h$ are the remainder terms as in Proposition 6.1 and

$$\begin{aligned} e_k^u &:= u - \widetilde{u}_k, & e_k^v &:= v - \widetilde{v}_k, & e_k^{z_1} &:= z_1 - \widetilde{z}_{1,k}, & e_k^{z_2} &:= z_2 - \widetilde{z}_{2,k}, \\ e_{kh}^u &:= u_k - \widetilde{u}_{kh}, & e_{kh}^v &:= v_k - \widetilde{v}_{kh}, & e_{kh}^{z_1} &:= z_{1,k} - \widetilde{z}_{1,kh}, & e_{kh}^{z_2} &:= z_{2,k} - \widetilde{z}_{2,kh}. \end{aligned}$$

Next, we split (6.11) and (6.12) into primal and dual residuals, where the remainder terms are neglected:

$$J(u,v) - J(u_k,v_k) \approx \frac{1}{2}\Big(\rho_u(u_k,v_k)(z_1 - \widetilde{z}_{1,k}) + \rho_u{}^*(u_k,v_k;z_{1,k},z_{2,k})(u-\widetilde{u}_k)\Big) \tag{6.13}$$
$$+\frac{1}{2}\Big(\rho_v(u_k,v_k)(z_2 - \widetilde{z}_{2,k}) + \rho_v{}^*(u_k,v_k;z_{1,k},z_{2,k})(v-\widetilde{v}_k)\Big),$$
$$J(u_k,v_k) - J(u_{kh},v_{kh}) \approx \frac{1}{2}\Big(\rho_u(u_{kh},v_{kh})(z_{1,k} - \widetilde{z}_{1,kh}) + \rho_u{}^*(u_{kh},v_{kh},z_{1,kh})(u_k-\widetilde{u}_{kh})\Big) \tag{6.14}$$
$$+\frac{1}{2}\Big(\rho_v(u_{kh},v_{kh})(z_{2,k} - \widetilde{z}_{2,kh}) + \rho_v{}^*(u_{kh},v_{kh};z_{1,kh},z_{2,kh})(v_k-\widetilde{v}_{kh})\Big),$$

The primal and dual residuals are defined as:

$$\rho_u(u,v)(\chi) := \widetilde{\mathcal{L}}'_{z_1}(u,v;z_1,z_2)(\chi), \quad \rho_u^*(u,v;z_1,z_2)(\varphi) := \widetilde{\mathcal{L}}'_u(u,v;z_1,z_2)(\varphi), \tag{6.15a}$$
$$\rho_v(u,v)(\xi) := \widetilde{\mathcal{L}}'_{z_2}(u,v;z_1,z_2)(\xi), \quad \rho_v^*(u,v;z_1,z_2)(\psi) := \widetilde{\mathcal{L}}'_v(u,v;z_1,z_2)(\psi) \tag{6.15b}$$

where $\widetilde{u}_k, \widetilde{v}_k, \widetilde{z}_{1,k}, \widetilde{z}_{2,k} \in \widetilde{X}_k^r$ and $\widetilde{u}_{kh}, \widetilde{v}_{kh}, \widetilde{z}_{1,kh}, \widetilde{z}_{2,kh} \in \widetilde{X}_{kh}^{s,r}$ can be chosen arbitrarily due to the Galerkin Orthogonality.

6.1.1 Dual equations

The explicit formulation for primal equations has been presented in (4.5). Here, we present the corresponding dual equations. We define the notation for the sum of the bilinear forms

$$a(u,v)(\varphi,psi) := a_1(u,v)(\varphi) + a_2(u,v)(\psi)\,.$$

The continuous dual solutions z_1, z_2 are the solutions of

$$J'(u,v)(\varphi,\psi) = (\partial_t\varphi, z_1) + a_1'(u)(\varphi,z_1,z_2) + a_2'(v)(\psi,z_1,z_2) + (\varphi(0), z_1(0)), \tag{6.17}$$

where the explicit forms are

$$\begin{aligned} ((\partial_t\varphi, z_1)) &= -((\partial_t z_1,\varphi)) + (z_1(T),\varphi(T)) - (\varphi(0),z_1(0)), \qquad (6.18)\\ a_1'(u)(\varphi,z_1,z_2) &= \alpha_2((\nabla z_1,\nabla\varphi)) - \alpha_5((z_2,\varphi)),\\ a_2'(v)(\psi,z_1,z_2) &= ((\nabla z_2,\nabla\psi)) + \alpha_4((z_2,\psi)) + \alpha_3((\nabla z_1,\nabla\psi)). \end{aligned}$$

For (6.18), we have integrated by parts, see, for instance, Wloka [75]. The fully discrete dual solutions $z_{1,kh}, z_{2,kh} \in \widetilde{X}_{kh}^{s,r}$ satisfy the equations

$$\sum_{m=1}^{M} \int_{I_m} (-\partial_t z_k, \varphi) + a_1'(u_{kh})(\varphi, z_1, z_2)\, dt + (z_{1,kh}^M, \varphi^M) + \sum_{m=0}^{M-1} ([z_{1,k}]_m, \varphi^-) + a_2'(v_{kh})(\psi, z_1, z_2)\, dt = \int_I J_1'(u_{kh}, v_{kh})(\varphi, \psi) + J_2'(u_{kh}^M, v_{kh}^M)(\varphi^M, \psi^M)\,.$$

6.2 Evaluation of the Error Estimators

The equations (6.13) and (6.14) are not yet useful since they contain the unknown continuous solutions u, v, z_1, z_2 and unknown semi-discrete solutions $u_k, v_k, z_{1,k}, z_{2,k}$. Based on the work of Schmich and Vexler[64], we further approximate these unknown solutions. Let w stand for u or v and z for z_1 or z_2. Because the quantities $\widetilde{w}_k, \widetilde{z}_k, \widetilde{w}_{kh}, \widetilde{z}_{kh}$ used in the weight factors can be chosen arbitrarily in the corresponding spaces, the weight factors $(w - \widetilde{w}_k), (z - \widetilde{z}_k), (w_k - \widetilde{w}_{kh}), (z_k - \widetilde{z}_{kh})$ in (6.13), (6.14) can be chosen as interpolation errors. In order to approximate the weights, we use a higher order interpolation for the continuous variables (see Bangerth and Rannacher [9] for its theoretical justification and for other possible interpolation methods). In this work, the following linear operators are chosen for the approximation error in time:

$$\begin{aligned} z - \widetilde{z}_k &\approx \Pi_k z_k, \\ w - \widetilde{w}_k &\approx \Pi_k w_k, \end{aligned}$$

and in space:

$$\begin{aligned} z_k - \widetilde{z}_{kh} &\approx \Pi_h z_{kh}, \\ w_k - \widetilde{w}_{kh} &\approx \Pi_h w_{kh}. \end{aligned}$$

In the case of the cG(1)dG(0) scheme,

$$\Pi_k : \widetilde{X}_{kh}^{0,1} \to X_{kh}^{1,1}, \quad \Pi_k := i_k^{(1)} - \mathrm{id},$$

and

$$\Pi_h : \widetilde{X}_{kh}^{0,1} \to \widetilde{X}_{kh}^{0,2}, \quad \Pi_h := i_{2h}^{(2)} - \mathrm{id}.$$

And in the case of the cG(1)cG(1) scheme, the linear operators Π_k and Π_h are defined by

$$\Pi_k : X_{kh}^{1,1} \to X_{kh}^{2,1} \cap C^0(I, V), \quad \Pi_k := i_{2k}^{(2)} - \mathrm{id}, \tag{6.19}$$

and

$$\Pi_h : X_{kh}^{1,1} \to X_{kh}^{1,2}, \qquad \Pi_h := i_{2h}^{(2)} - \mathrm{id}$$

where "id" is the identity function, and the piecewise linear operators, $i_k^{(1)}$ and $i_{2k}^{(2)}$, are defined as

$$i_k^{(1)} v(t) := \frac{t_m - t}{k_m} v(t_{m-1}) + \frac{t - t_{m-1}}{k_m} v(t_m), \quad t \in (t_{m-1}, t_m], \tag{6.20}$$

$$\begin{aligned} i_{2k}^{(2)} v(t) := {} & \frac{(t_m - t)(t_{m+1} - t)}{k_m(k_m + k_{m+1})} v(t_{m-1}) + \frac{(t - t_{m-1})(t_{m+1} - t)}{k_m k_{m+1}} v(t_m) \\ & + \frac{(t - t_{m-1})(t - t_m)}{k_m(k_m + k_{m+1})} v(t_{m+1}), \quad t \in (t_{m-1}, t_{m+1}], \end{aligned} \tag{6.21}$$

as seen in Figure 6.1.

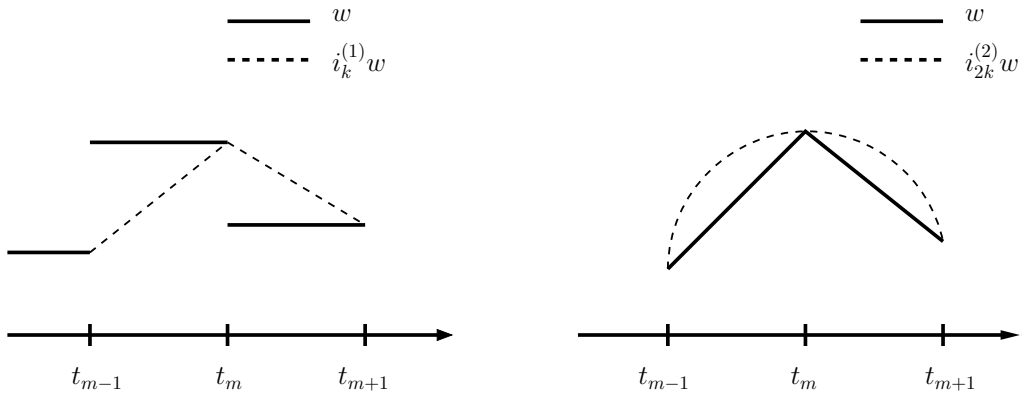

Figure 6.1. Piecewise linear interpolation(left) and piecewise quadratic interpolation(right) in dotted line.

For the case of the damped Crank-Nicolson scheme, for one or more first damping steps, the implicit Euler scheme is applied to ensure the convergence. An example of the interpolation for the damped scheme is found in Figure 6.2 where only one implicit Euler step is applied.

The next step of approximation is to replace all the unknown semi-discrete terms w_k, z_k in the residual equations (6.13), (6.14) with the fully discrete solutions w_{kh}, z_{kh}. We derive the residuals,

$$J(u, v) - J(u_{kh}, v_{kh}) \approx \eta_k^u + \eta_k^v + \eta_h^u + \eta_h^v \tag{6.22}$$

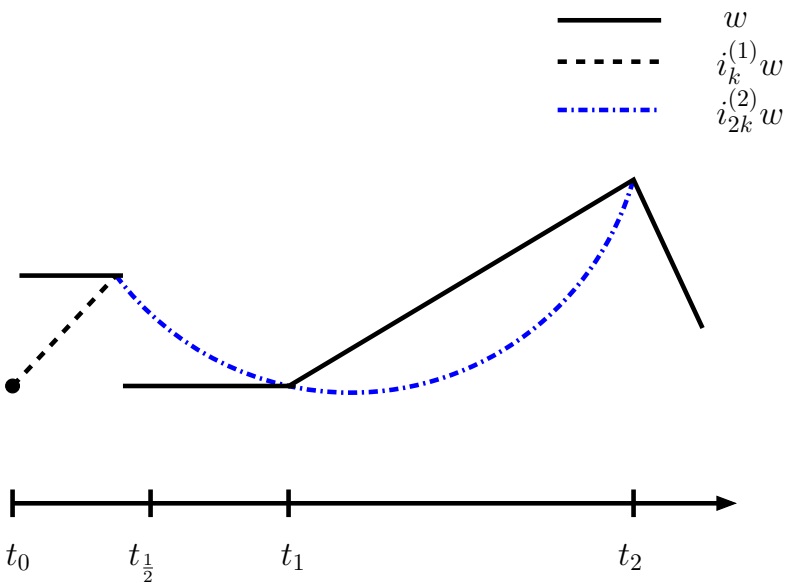

Figure 6.2. An example of the interpolation for the damped Crank-Nicolson scheme, where the first step is taken by the implicit Euler scheme.

where each error estimator is written as

$$\eta_k^u := \frac{1}{2}\left(\rho_u(u_{kh}, v_{kh})(\Pi_k z_{1,kh}) + \rho_u^*(u_{kh}, v_{kh}; z_{1,kh}, z_{2,kh})(\Pi_k u_{kh})\right), \quad (6.23a)$$

$$\eta_k^v := \frac{1}{2}\left(\rho_v(u_{kh}, v_{kh})(\Pi_k z_{2,kh}) + \rho_v^*(u_{kh}, v_{kh}; z_{1,kh}, z_{2,kh})(\Pi_k v_{kh})\right), \quad (6.23b)$$

$$\eta_h^u := \frac{1}{2}\left(\rho_u(u_{kh}, v_{kh})(\Pi_h z_{1,kh}) + \rho_u^*(u_{kh}, v_{kh}; z_{1,kh}, z_{2,kh})(\Pi_h u_{kh})\right), \quad (6.23c)$$

$$\eta_h^v := \frac{1}{2}\left(\rho_v(u_{kh}, v_{kh})(\Pi_h z_{2,kh}) + \rho_v^*(u_{kh}, v_{kh}; z_{1,kh}, z_{2,kh})(\Pi_h v_{kh})\right). \quad (6.23d)$$

Remark 6.1. It is crucial for an efficient adaptive algorithm that η_k and η_h are completely independent of each other, i.e., refinement of spatial discretization is not influenced by η_k and vice versa. This independence is important, otherwise the spatial error indicator would decrease on refining the temporal discretization, even if the spatial discretization is fixed.

Remark 6.2. Instead of approximating the unknown semi-discrete solutions by fully discrete solutions, one can use a higher-order interpolation in space , as done for the weight factors. For the details, refer Meidner [49], Schmich and Vexler [64].

6.3 Localization of the Error Estimators

One of the main purposes of the a posteriori error estimators developed in the previous section is to assess the discretization error so that we can adaptively adjust the discretizations in order to efficiently improve the accuracy. Therefore, we further localize the error estimators to cell-wise contributions. These localized quantities are then called *local error indicators*. Thus, the overall error estimators are split into their contributions on each subinterval I_m,

$$\eta_k = \sum_{m=1}^{M} \eta_k^m \quad \text{and} \quad \eta_h = \sum_{m=0}^{M} \eta_h^m. \tag{6.24}$$

The contribution η_k^m can be used for an adaptive refinement of the temporal discretizations.

The spatial contributions can be localized further on each cell of the mesh. The resulting local error contains the strong residual of the equation, as well as jumps of the discrete solution over the faces of the cells (as shown explicitly in the next section).
Let K be a cell in a mesh T_h, then we can further localize the error indicator for each time step η_h^m into each cell,

$$\eta_h^m = \sum_{K \in T_h} \eta_{h|K}^m.$$

In the DWR method, the residual is integrated by parts to attain the oscillatory behavior of the residuals such that the cell-wise contributions of the residuals are evaluated by the corresponding cell and its surrounding edges. The edge shared by two cells, K and its neighboring cell $K^{'}$ is denoted as $\Gamma = K \cap K^{'}$. Also, the jump of the normal derivative of u from a cell K to $K^{'}$ over Γ is

$$[\partial_n u] = [n \cdot \nabla u] := n \cdot (\nabla u_{h|K \cap \Gamma} - \nabla u_{h|K' \cap \Gamma}), \tag{6.25}$$

where n is the outer unit normal vector. Then we replace the term $((\nabla u^m, \nabla \varphi))$ in local and dual residual with

$$((\nabla u^m, \nabla \varphi)) = \sum_{K \in T_h} \int_{I_m} (-\Delta u^m, \varphi)_K + \frac{1}{2} ([n \cdot \nabla u^m], \varphi)_{\partial K \setminus \partial \Omega}$$

where the homogeneous Dirichlet boundary condition is applied on the boundary. $\frac{1}{2}$ on the right-hand side is derived by the jump between two cells, which occurs once from both neighboring cells.

6.4 Error Estimators for the System

In this section, we present the explicit formulations of the approximated error estimators. These are separated into eight parts, for primal and dual residuals in time and space discretizations for the two sub-parts of the system. We present the estimators for the implicit Euler scheme and for the Crank-Nicolson scheme. Note that we use the homogeneous Dirichlet boundary condition on the boundary. Here, for the fully discrete solutions, we use the notation for the simplicity as follows:

$$u := u_{kh}, \quad v := v_{kh}, \quad z_1 := z_{1,kh}, \quad z_2 := z_{2,kh}$$

6.4.1 Error estimators for cG(1)dG(0)

For the implicit Euler method, the temporal integrals involving the fully discrete solutions, u, v, z_1 and z_2 are approximated by the box rule, whereas those involving $i_k^{(1)}$ and the right-hand-side terms with f, g, are evaluated by the trapezoidal rule. The residuals are as follows:

For the estimate in time for the parabolic equation η_k^u, we use the piecewise linear interpolation (6.20), and localize into each subintervals in time I_m. Then, the primal residual is:

$$\begin{aligned}\rho_u(u,v)(\Pi_k z_1) = ((f, \Pi_k z_1)) - \sum_{m=1}^{M} \int_{I_m} (\partial_t u^m, \Pi_k z_1(t))\ dt - a_1(u^m, v^m)(\Pi_k z_1(t)) \\ - \sum_{m=0}^{M-1} ([u]_m, \Pi_k z_1^{m,+}) - (u(0)^- - u_0, z_1(0)^-)\,.\end{aligned}$$

Using the interpolation defined in (6.20), we know that

$$\Pi_k z_1(t) = \frac{t - t_m}{k_m}(z_1^m - z_1^{m-1})$$

on the interval I_m. Also $\Pi_k z_1^{m,+} = z_1^m - z_1^{m+1}$ and $[u]_m = u^{m+1} - u^m$. After re-indexing on the summations to merge under one summation, we have

$$\begin{aligned}\rho_u(u,v)(\Pi_k z_1) = \sum_{m=1}^{M} \Bigg[\left(u^m - u^{m-1}, z_1^m - z_1^{m-1}\right) + \int_{I_m} \frac{t - t_m}{k_m} \left(f, z_1^m - z_1^{m-1}\right) dt \\ + \frac{k_m}{2} \left(\alpha_2 \nabla u^m + \alpha_3 \nabla v^m, \nabla \left(z_1^m - z_1^{m-1}\right)\right) \Bigg] - (u^0 - u_0, z_1^1 - z_1^0).\end{aligned}$$

Note that $\partial_t u = 0$ because u_{kh} is constant on each interval I_m for the implicit Euler method. Also, the linear interpolations are integrated over time by the trapezoidal rule and produce the term $\frac{k_m}{2}$. To discretize further into cell-wise, we use the integration by parts and apply the homogeneous Dirichlet boundary condition, from which we obtain:

$$\begin{aligned}\rho_u(u,v)(\Pi_k z_1) = \sum_{m=1}^{M}\Bigg[\sum_{K\in T_h}\Bigg\{&\left(u^m-u^{m-1}, z_1^m - z_1^{m-1}\right)_K - \frac{k_m}{2}\left(f^{m-1}, z_1^m - z_1^{m-1}\right)_K\\ &- \frac{k_m}{2}\left(\alpha_3 \Delta v^m + \alpha_2 \Delta u^m, z_1^m - z_1^{m-1}\right)_K\\ &+ \frac{k_m}{4}\left(\alpha_2[\partial_n u^m] + \alpha_3[\partial_n v^m], z_1^m - z_1^{m-1}\right)_{\partial K\setminus\partial\Omega}\Bigg\}\Bigg]\\ &- (u^0 - u_0, z_1^1 - z_1^0).\end{aligned}$$

Here, $[\partial_n u^m]$ is the jump term between cells K as defined as in (6.25) (do not confuse with the jump term $[u]_m$ in (4.1)). Note that $z_1^1 = z_1^0$ because the dual equation is solved backward in time. Next, the dual residual in time for the parabolic equation derived from $\mathcal{L}'_{z_1}(u,z_1)(\Pi_k z_1)$ is:

$$\begin{aligned}\rho_u^*(u,v;z_1,z_2)(\Pi_k u) &= J'_u(u)(\Pi_k u) + \sum_{m=1}^{M}\int_{I_m}(\Pi_k u(t), \partial_t z_1^m)\,dt - (\Pi_k u^M, z_1^M)\\ &\quad + (\Pi_k u^0, z_1^0) - a_1'(u^m, v^m)(\Pi_k u(t), z_1^m) - \sum_{m=0}^{M-1}(\Pi_k u(t_m)^-, [z_1]_m)\\ &\quad - (\Pi_k u(0)^-, z_1(0)^-)\\ &= \sum_{m=1}^{M}\Bigg[\frac{\alpha_2 k_m}{2}\left(\nabla\left(u^m - u^{m-1}\right), \nabla z_1^m\right) - \frac{\alpha_5 k_m}{2}\left(u^m - u^{m-1}, z_2^m\right)\\ &\quad - \frac{k_m}{2}J'_{1,u}(u^m)(u^m - u^{m-1})\Bigg] + J'_{2,u}(u^M)(\underbrace{(i_k^{(1)} - \mathrm{id})u^M}_{=0})\\ &\quad - (\underbrace{(i_k^{(1)} - \mathrm{id})u^M}_{=0}, z_1^M).\end{aligned}$$

Here, $\partial_t z_1^m = 0$ and $(\Pi_k u(t_m)^-) = 0$. Now we split it further into the contribution from each cell and include the terms for interfaces between cells and boundary. (The

terms with zero boundary condition applied are not shown.)

$$\begin{aligned}\rho_u^*(u,v;z_1,z_2)(\Pi_k u) = \sum_{m=1}^{M}\Bigg[\sum_{K\in T_h}\Bigg\{&\frac{\alpha_2 k_m}{2}\left(\left(u^m-u^{m-1}\right),-\Delta z_1^m\right)_K\\ &+\frac{\alpha_2 k_m}{4}\left(u^m-u^{m-1},[\partial_n z_1^m]\right)_{\partial K\setminus\partial\Omega}\\ &-\frac{\alpha_5 k_m}{2}(u^m-u^{m-1},z_2^m)_K-\frac{k_m}{2}J'_{1,u}(u^m)(u^m-u^{m-1})_K\Bigg\}\Bigg]\end{aligned}$$

Analogously, for the estimate for the elliptic equation η_k^v, we derive the primal residual in time as:

$$\begin{aligned}\rho_v(u,v)(\Pi_k z_2) = \sum_{m=1}^{M}\Bigg[\sum_{K\in T_h}\Bigg\{&-\frac{k_m}{2}\left(\Delta v^m,z_2^m-z_2^{m-1}\right)_K-\frac{k_m}{2}\left(g^{m-1},z_2^m-z_2^{m-1}\right)_K\\ &+\frac{k_m}{4}\left([\partial_n v^m],z_2^m-z_2^{m-1}\right)_{\partial K\setminus\partial\Omega}\\ &+\frac{k_m}{2}\left(\alpha_4 v^m-\alpha_5 u^m,z_2^m-z_2^{m-1}\right)_K\Bigg\}\Bigg],\end{aligned}$$

and the dual residual in time as:

$$\begin{aligned}\rho_v^*(u,v;z_1,z_2)(\Pi_k v) = \sum_{m=1}^{M}\Bigg[\sum_{K\in T_h}\Bigg\{&\frac{\alpha_3 k_m}{2}\left(\nabla\left(v^m-v^{m-1}\right),\nabla z_1^m\right)_K\\ &+\frac{k_m}{2}\left(v^m-v^{m-1},-\Delta z_2^m\right)_K+\frac{k_m}{4}\left(v^m-v^{m-1},[\partial_n z_2^m]\right)_{\partial K\setminus\partial\Omega}\\ &+\frac{\alpha_4 k_m}{2}(v^m-v^{m-1},z_2^m)_K-\frac{k_m}{2}J'_{1,v}(v^m)(v^m-v^{m-1})_K\Bigg\}\Bigg]\\ &+J'_{2,v}(v^M)(\Pi_k v^M).\end{aligned}$$

For the estimate in space η_h^u, we use the piecewise quadratic interpolation defined

previously (6.21). The primal residual in space of the parabolic equation is:

$$\begin{aligned}\rho_u(u,v)(\Pi_h z_1) = \sum_{m=1}^{M}\Bigg[\sum_{K\in T_h}\Bigg\{\int_{I_m}\left(f(t), i_{2h}^{(2)}z_1(t) - z_1^m\right)_K dt \\ + k_m\left(\alpha_2\Delta u^m + \alpha_3\Delta v^m, i_{2h}^{(2)}z_1(t) - z_1^m\right)_K \\ - \left(u^m - u^{m-1}, i_{2h}^{(2)}z_1(t) - z_1^m\right)_K \\ - \frac{k_m}{2}\left(\alpha_2[\partial_n u^m] + \alpha_3[\partial_n v^m], i_{2h}^{(2)}z_1(t) - z_1^m\right)_{\partial K\setminus\partial\Omega}\Bigg\} \\ - \left(u^0 - u_0, i_{2h}^{(2)}z_1^0 - z_1^0\right),\end{aligned}$$

and the dual residual in space is:

$$\begin{aligned}\rho_u^*(u,v;z_1,z_2)(\Pi_h u) = \sum_{m=1}^{M}\Bigg[\sum_{K\in T_h}\Big\{k_m J'_{1,u}(u^m)(i_{2h}^{(2)}u(t) - u^m)_K \\ + \alpha_2 k_m\left(i_{2h}^{(2)}u(t) - u^m, \Delta z_1^m\right)_K + \alpha_5 k_m\left(i_{2h}^{(2)}u(t) - u^m, z_2^m\right)_K \\ - \frac{\alpha_2 k_m}{2}\left(i_{2h}^{(2)}u(t) - u^m, [\partial_n z_1^m]\right)_{\partial K\setminus\partial\Omega} \\ + (i_{2h}^{(2)}u(t)\mid_{m-1} - u^{m-1}, z_1^m - z_1^{m-1})_K\Big\}\Bigg] \\ + J'_{2,u}(u^M)(i_{2h}^{(2)}u^M - u^M) - (i_{2h}^{(2)}u^M - u^M, z_1^M).\end{aligned}$$

Note that the quadratic interpolations are not explicitly calculated out as they are for the linear interpolations.
Finally, the primal and dual residuals for the elliptic equations for η_h^v are:

$$\begin{aligned}\rho_v(u,v)(\Pi_h z_2) = \sum_{m=1}^{M}\Bigg[\sum_{K\in T_h}\Big\{k_m\left(\Delta v^m, i_{2h}^{(2)}z_2(t) - z_2^m\right)_K \\ + \int_{I_m}\left(g(t), i_{2h}^{(2)}z_2(t) - z_2^m\right)_K dt - \frac{k_m}{2}\left([\partial_n v^m], i_{2h}^{(2)}z_2(t) - z_2^m\right)_{\partial K\setminus\partial\Omega} \\ + k_m\left(\alpha_5 u^m - \alpha_4 v^m, i_{2h}^{(2)}z_2(t) - z_2^m\right)_K dt\Big\}\Bigg],\end{aligned}$$

and

$$\begin{aligned}\rho_v^*(u,v;z_1,z_2)(\Pi_h v) = \sum_{m=1}^{M}\Bigg[\sum_{K\in T_h}\Big\{&k_m J'_{1,v}(v^m)(i_{2h}^{(2)}v(t)-v^m)_K\\ &-k_m\left(i_{2h}^{(2)}v(t)-v^m,-\Delta z_2^m\right)_K\\ &-\alpha_3 k_m\left(\nabla(i_{2h}^{(2)}v(t)-v^m),\nabla z_1^m\right)_K\\ &-\frac{k_m}{2}\left(i_{2h}^{(2)}v(t)-v^m,[\partial_n z_2^m]\right)_{\partial K\setminus\partial\Omega}\\ &-\alpha_4 k_m\left(i_{2h}^{(2)}v(t)-v^m,z_2^m\right)_K\Big\}\Bigg]+J'_{2,v}(v^M)(i_{2h}^{(2)}v^M-v^M).\end{aligned}$$

6.4.2 Error estimators for cG(1)cG(1)

Since we have right-hand sides that are time-dependent trigonometric functions, we use the Gaussian quadrature for the integration method for more accurate integration than that which we would derive from the trapezoidal rule.
We present here the primal residual of the parabolic equation:

$$\begin{aligned}\rho_u(u,v)(\Pi_k z_1) = \sum_{m=1}^{M}\int_{I_m}&\underbrace{(f(t),\Pi_k z1(t))}_{(1)}-\underbrace{(\partial_t u^m,\Pi_k z1(t))}_{(2)}-\alpha_2\underbrace{(\nabla u^m,\nabla\Pi_k z1(t))}_{(3)}\\ &-\alpha_3\underbrace{(\nabla v^m,\nabla\Pi_k z1(t))}_{(4)}\,dt-(u(0)-u_0,z_1(0))\,.\end{aligned}$$

Let

$$x_1 := \frac{k_m}{2\sqrt{3}}+\frac{t_m+t_{m-1}}{2},\quad x_2 := -\frac{k_m}{2\sqrt{3}}+\frac{t_m+t_{m-1}}{2}\,. \tag{6.28}$$

The approximation by Gaussian Quadrature of the four terms in (6.28) is:

$$\begin{aligned}(1)\quad\int_{I_m}(f,\Pi_k z_1)\,dt &= \int_{I_m}\left(f(t),\frac{t_m-t}{k_m}z_1^{m-1}+\frac{t-t_{m-1}}{k_m}z_1^m-z_1^m\right)dt\\ &\approx \frac{k_m}{2}\left(f(x_1),\frac{t_m-x_1}{k_m}z_1^{m-1}+\frac{x_1-t_{m-1}}{k_m}z_1^m-z_1^m\right)\\ &\quad+\frac{k_m}{2}\left(f(x_2),\frac{t_m-x_2}{k_m}z_1^{m-1}+\frac{x_2-t_{m-1}}{k_m}z_1^m-z_1^m\right),\end{aligned}$$

Note the right-hand side is also time dependent.

$$
\begin{aligned}
(2) \quad \int_{I_m} (\partial_t u, \Pi_k z_1)\, dt &= \int_{I_m} \left(\frac{u^m - u^{m-1}}{k_m}, \frac{t_m - t}{k_m} z_1^{m-1} + \frac{t - t_{m-1}}{k_m} z_1^m - z_1^m \right) dt \\
&\approx \frac{k_m}{2} \left(\frac{u^m - u^{m-1}}{k_m}, \frac{t_m - x_1}{k_m} z_1^{m-1} + \frac{x_1 - t_{m-1}}{k_m} z_1^m - z_1^m \right) \\
&\quad + \frac{k_m}{2} \left(\frac{u^m - u^{m-1}}{k_m}, \frac{t_m - x_2}{k_m} z_1^{m-1} + \frac{x_2 - t_{m-1}}{k_m} z_1^m - z_1^m \right),
\end{aligned}
$$

$$
\begin{aligned}
(3) \quad \int_{I_m} (\nabla u(t), \Pi_k \nabla z_1)\, dt &= \int_{I_m} \left(\frac{t_m - t}{k_m} \nabla u^{m-1} + \frac{t - t_{m-1}}{k_m} \nabla u^m, \right. \\
&\quad \left. \frac{t_m - t}{k_m} \nabla z_1^{m-1} + \frac{t - t_{m-1}}{k_m} \nabla z_1^m - \nabla z_1^m \right) dt.
\end{aligned}
$$

In this term (3), we use the distribution property for the product within the integral and obtain:

$$
\begin{aligned}
\int_{I_m} (\nabla u^m, \Pi_k \nabla z_1^m)\, dt &= \int_{I_m} \left(\frac{t_m - t}{k_m} \right)^2 (\nabla u^{m-1}, \nabla z_1^{m-1})\, dt \\
&\quad + \int_{I_m} \left(\frac{t_m - t}{k_m} \right) \left(\frac{t - t_{m-1}}{k_m} \right) \left(\nabla u^{m-1}, \nabla z_1^m \right) dt \\
&\quad + \int_{I_m} \left(\frac{t_m - t}{k_m} \right) \left(\frac{t - t_{m-1}}{k_m} \right) \left(\nabla u^m, \nabla z_1^{m-1} \right) dt \\
&\quad - \int_{I_m} \left(\frac{t_m - t}{k_m} \right) (\nabla u^{m-1}, \nabla z_m) + \left(\frac{t - t_{m-1}}{k_m} \right)^2 (\nabla u^m, \nabla z_1^m)\, dt \\
&\quad - \int_{I_m} \left(\frac{t - t_{m-1}}{k_m} \right) (\nabla u^m, \nabla z_1^m)\, dt =: \int_{t_{m-1}}^{t_m} h(t)\, dt\,.
\end{aligned}
$$

The integral over $[t_{m-1}, t_m]$ must be changed into an integral over $[-1, 1]$ before applying the Gaussian quadrature rule. This change of interval can be done and the

term (3) is written as:

$$\begin{aligned}\int_{I_m} (\nabla u(t), \Pi_k \nabla z_1^m)\, dt &= \frac{k_m}{2} \int_{-1}^{1} h\left(\frac{k_m}{2}x + \frac{t_m + t_{m-1}}{2}\right) dx \\ &=: \int_{-1}^{1} g(x)dx \quad \approx g\left(\frac{1}{\sqrt{3}}\right) + g\left(\frac{-1}{\sqrt{3}}\right) \\ &= \frac{k_m}{2}\left[h\left(x_1\right) + h\left(x_2\right)\right],\end{aligned}$$

Similarly,

$$\begin{aligned}(4) \quad \int_{I_m} (\nabla v(t), \Pi_k \nabla z_1)\, dt = &\int_{I_m} \left(\frac{t_m - t}{k_m}\right)^2 \left(\nabla v^{m-1}, \nabla z_1^{m-1}\right) dt \\ &+ \int_{I_m} \left(\frac{t_m - t}{k_m}\right)\left(\frac{t - t_{m-1}}{k_m}\right) \left(\nabla v^{m-1}, \nabla z_1^{m}\right) dt \\ &+ \int_{I_m} \left(\frac{t_m - t}{k_m}\right)\left(\frac{t - t_{m-1}}{k_m}\right) \left(\nabla v^{m}, \nabla z_1^{m-1}\right) dt \\ &- \int_{I_m} \left(\frac{t_m - t}{k_m}\right) \left(\nabla v^{m-1}, \nabla z^{m}\right) \\ &+ \left(\frac{t - t_{m-1}}{k_m}\right)^2 (\nabla v^m, \nabla z_1^m)\, dt \\ &- \int_{I_m} \left(\frac{t - t_{m-1}}{k_m}\right) (\nabla v^m, \nabla z_1^m)\, dt\,.\end{aligned}$$

6.5 Estimation of Galerkin Perturbation Error

The computed a posteriori error estimators in the previous sections are effective criteria for developing the refinement algorithm. However, these estimators are generated for the "exact" discrete solutions. In our case, due to the splitting method, we use inexact intermediate solutions. Thus, we must consider an additional error from the multirate iterative coupling scheme introduced in Chapter 5.

6.5.1 Splitting error estimation

The weak formulation (3.1) can be stated using (3.2) as:
Find $u, v \in X$ such that

$$\mathcal{A}(u,v)(\varphi,\psi) = 0, \quad \forall \varphi,\psi \in X. \tag{6.29}$$

We discretize the problem by a standard finite element method in time and space and write the fully discrete problem:
Find $u_{kh}, v_{kh} \in \widetilde{X}_{kh}^{r,s}$ such that

$$\mathcal{A}(u_{kh},v_{kh})(\varphi,\psi) = 0, \quad \forall \varphi,\psi \in \widetilde{X}_{kh}^{r,s}. \tag{6.30}$$

Assuming the Equation (6.30) is solved exactly, the a posteriori error estimates for $(u - u_{kh})$ and $(v - v_{kh})$ are derived as in the previous section.
However, due to the inexact intermediate solutions $\widetilde{u}_{kh}$,$\widetilde{v}_{kh}$ from the splitting method, we violate the Galerkin orthogonality. This violation is called the Galerkin perturbation. Let us denote the estimate of the error due to this Galerkin perturbation as η_{pert}. We define the function spaces $\bar{X}_{kh}^{r,s}$, $\bar{Y}$ and Y as defined in (6.5) and (6.10), respectively, so that they satisfy that $\bar{X}_{kh}^{r,s} \subset \bar{Y}$. Then, there holds the following proposition:

Proposition 6.2. *Let $(\widetilde{u}_{kh}, \widetilde{v}_{kh}; \widetilde{z}_{1,kh}, \widetilde{z}_{2,kh}) \in \bar{X}_{kh}^{r,s}$ be the approximated primal and dual solutions $(u, v; z_1, z_2) \in \bar{Y}$ of (3.1) and (6.17). Then the error representation holds:*

$$\begin{aligned} J(u,v) - J(\widetilde{u}_{kh},\widetilde{v}_{kh}) &= \eta_k^{u+v}(\widetilde{u}_{kh},\widetilde{v}_{kh};\widetilde{z}_{1,kh},\widetilde{z}_{2,kh}) + \eta_h^{u+v}(\widetilde{u}_{kh},\widetilde{v}_{kh};\widetilde{z}_{1,kh},\widetilde{z}_{2,kh}) \\ &+ \eta_{pert} + \mathcal{R}^{(3)}, \end{aligned}$$

where

$$\begin{aligned} \eta_{pert} &= \eta_{pert}^u + \eta_{pert}^v \\ &:= \rho_u(\widetilde{u}_{kh},\widetilde{v}_{kh})(\widetilde{z}_{1,kh}) + \rho_v(\widetilde{u}_{kh},\widetilde{v}_{kh})(\widetilde{z}_{2,kh}) \end{aligned} \tag{6.31}$$

and $\mathcal{R}^{(3)}$ is cubic in the primal and dual errors.

Proof. We define $\omega := \{u, v; z_1, z_2\}$ and $\widetilde{\omega}_{kh} := \{\widetilde{u}_{kh}, \widetilde{v}_{kh}; \widetilde{z}_{1,kh}, \widetilde{z}_{2,kh}\}$. By applying the mean value theorem and the fundamental theorem of calculus, followed by a change of variables on the Lagrangian (6.6), there holds

$$\mathcal{L}(\omega) - \mathcal{L}(\widetilde{\omega}_{kh}) = \int_0^1 \mathcal{L}'(\widetilde{\omega}_{kh} + s(e))(e)\, ds,$$

where $e = \omega - \widetilde{\omega}_{kh}$. With the general error representation for the trapezoidal rule

$$\int_0^1 f(s)\, ds = \frac{1}{2}\left(f(0) + f(1)\right) + \frac{1}{2}\int_0^1 f''(s)s(s-1)\, ds,$$

we use the fact that $\mathcal{L}'(\omega) = 0$ and derive that

$$\mathcal{L}(\omega) - \mathcal{L}(\widetilde{\omega}_{kh}) = \frac{1}{2}\mathcal{L}'(\widetilde{\omega}_{kh})(e) + \mathcal{R}^{(3)}, \tag{6.34}$$

where $\mathcal{R}^{(3)}$ is cubic in the primal and dual errors as in [60]. Then, we recall (6.29) and write the error functional as

$$\begin{aligned} J(u,v) - J(\widetilde{u}_{kh}, \widetilde{v}_{kh}) &= \mathcal{L}(\omega) + \mathcal{A}(u,v)(z_1, z_2) - \mathcal{L}(\widetilde{\omega}_{kh}) - \mathcal{A}(\widetilde{u}_{kh}, \widetilde{v}_{kh})(\widetilde{z}_{1,kh}, \widetilde{z}_{2,kh}) \\ &= \mathcal{L}(\omega) - \mathcal{L}(\widetilde{\omega}_{kh}) - \mathcal{A}(\widetilde{u}_{kh}, \widetilde{v}_{kh})(\widetilde{z}_{1,kh}, \widetilde{z}_{2,kh}) \\ &= \frac{1}{2}\mathcal{L}'(\widetilde{\omega}_{kh})(e) + \mathcal{R}^{(3)} - \mathcal{A}(\widetilde{u}_{kh}, \widetilde{v}_{kh})(\widetilde{z}_{1,kh}, \widetilde{z}_{2,kh}) \end{aligned}$$

The proof is completed by recalling (6.15) and (6.23). □

This proof is adapted from the work of Rannacher and Vihharev [60] for the space-discrete equations for the nonlinear elliptic problems. They assess the error due to an inexact solution. This error is commonly called *iteration error* for stationary problems [58, 62].

6.5.2 Quadrature error

In his work, Strang [67] explained four sources of error contributions in η_{pert} due to the *variational crime*. Since the time integral in the variational formulation of the system (6.30) is not computed exactly, η_{pert} contains another error, in addition to the splitting error. In our calculation, we observe that this second error occurs if the residuals are evaluated by numerical quadrature, rather than exact integration; we call this additional error the *quadrature error*.
We begin this subsection with a focus on deriving the quadrature error through considering it with the exact solutions $u_{kh}, v_{kh}, z_{1,kh}, z_{2,kh}$.

We consider the perturbed bilinear form $\mathcal{A}_h$, where the integrals are integrated by a quadrature rule. From this, we know that

$$\mathcal{A}_h(u_{kh}, v_{kh})(\varphi, \psi) = 0 \quad \forall \varphi, \psi \in \widetilde{X}_{kh}^{r,s}. \tag{6.35}$$

By the First Lemma of Strang [14], with the notation $x := \{u, v\} \in Y \times Y$, $x_{kh} := \{u_{kh}, v_{kh}\} \in X_{kh}^{r,s} \times X_{kh}^{r,s} := S$,

$$||x - x_{kh}|| \leq c \left(\inf_{\Psi \in S} \left\{ ||x - \Psi|| + \sup_{\Phi \in S} \frac{|\mathcal{A}(u_{kh}, v_{kh})(\Phi) - \mathcal{A}_h(u_{kh}, v_{kh})(\Phi)|}{||\Phi||} \right\} \right)$$

for some constant c independent of discretizations. Then we know that the second term on the right-hand side is non zero and describes the quadrature error.
We consider the residuals defined as:

$$\begin{aligned} \rho_u(u, v)(z_1) &= ((f, z_1)) - \sum_{m=1}^{M} \int_{I_m} (\partial_t u, z_1)\, dt - a_1(u)(z_1), \\ \rho_v(u, v)(z_2) &= ((g, z_2)) - a_2(v)(z_2). \end{aligned}$$

We compute these residuals for the fully discrete solutions by using a Gaussian quadrature with a sufficiently high order to integrate the trigonometric functions f, g more precisely, and denote them as

$$\rho_u^{G.Q}(u_{kh}, v_{kh})(z_{1,kh}) \quad \text{and} \quad \rho_v^{G.Q}(u_{kh}, v_{kh})(z_{2,kh}).$$

Then,

$$\eta_{pert}^u = \rho_u^{G.Q}(u_{kh}, v_{kh})(z_{1,kh}), \tag{6.36a}$$

$$\eta_{pert}^v = \rho_v^{G.Q}(u_{kh}, v_{kh})(z_{2,kh}). \tag{6.36b}$$

On the other hand, since u_{kh}, v_{kh} are the solutions of the perturbed problem with $\mathcal{A}_h$ (6.35), the perturbed residuals are integrated by the trapezoidal rule:

$$\begin{aligned} \rho_u^{trapz}(u_{kh}, v_{kh})(z_{1,kh}) = \sum_{m=1}^{M} \Bigg[& \frac{k_m}{2} \left(f^m + f^{m-1}, z_{1,kh}^m \right) + \left(u_{kh}^m - u_{kh}^{m-1}, z_{1,kh}^m \right) \\ & - \frac{k_m}{2} \left(\alpha_2 \nabla u_{kh}^m + \alpha_3 \nabla v_{kh}^m, \nabla z_{1,kh}^m \right) \\ & - \frac{k_m}{2} \left(\alpha_2 \nabla u_{kh}^{m-1} + \alpha_3 \nabla v_{kh}^{m-1}, \nabla z_{1,kh}^m \right) \Bigg] - (u_{kh}^0 - u_0, z_{1,kh}^m), \\ \rho_v^{trapz}(u_{kh}, v_{kh})(z_{2,kh}) = \sum_{m=1}^{M} \Bigg[& \left(g^m + g^{m-1}, z_{2,kh}^m \right) - \left(\nabla v_{kh}^m + \nabla v_{kh}^{m-1}, \nabla z_{2,kh}^m \right) \\ & - \left(\alpha_4 v_{kh}^m - \alpha_5 u_{kh}^m, z_{2,kh}^m \right) - \left(\alpha_4 v_{kh}^{m-1} - \alpha_5 u_{kh}^{m-1}, z_{2,kh}^m \right) \Bigg], \end{aligned}$$

where $f^m := f(t_m)$ and $g^m := g(t_m)$.

Now we combine the results from the previous subsection 6.5.1, where we derive the Galerkin perturbation error due to using the approximated solutions $\widetilde{u}_{kh}, \widetilde{v}_{kh}, \widetilde{z}_{1,kh}, \widetilde{z}_{2,kh}$ in the splitting method. We would like to separate the perturbation error estimate into the error contribution from the splitting error η_{split}, and the quadrature error η_{quad}:

$$\eta_{pert} = \eta_{quad} + \eta_{split}. \tag{6.37}$$

We denote these estimates as

$$\eta^u_{quad} := \rho^{G.Q}_u(\widetilde{u}_{kh}, \widetilde{v}_{kh})(\widetilde{z}_{1,kh}) - \rho^{trapz}_u(\widetilde{u}_{kh}, \widetilde{v}_{kh})(\widetilde{z}_{1,kh}), \tag{6.38a}$$
$$\eta^v_{quad} := \rho^{G.Q}_v(\widetilde{u}_{kh}, \widetilde{v}_{kh})(\widetilde{z}_{2,kh}) - \rho^{trapz}_v(\widetilde{u}_{kh}, \widetilde{v}_{kh})(\widetilde{z}_{2,kh}). \tag{6.38b}$$

The splitting error is nothing but ρ^{trapz} because for the exact fully discrete solutions solved by using the Crank-Nicolson time scheme, it holds that

$$\rho^{trapz}_u(u_{kh}, v_{kh})(z_{1,kh}) = 0.$$

Therefore, we can denote the splitting error as:

$$\eta^u_{split} := \rho^{trapz}_u(\widetilde{u}_{kh}, \widetilde{v}_{kh})(\widetilde{z}_{1,kh}), \tag{6.40a}$$
$$\eta^v_{split} := \rho^{trapz}_v(\widetilde{u}_{kh}, \widetilde{v}_{kh})(\widetilde{z}_{2,kh}). \tag{6.40b}$$

However, for instance, for the approximated solutions

$$\rho^{trapz}_u(\widetilde{u}_{kh}, \widetilde{v}_{kh})(\widetilde{z}_{1,kh}) \neq 0\,,$$

implies that this error catches the splitting error.
In this thesis, we have the time-dependent trigonometric functions f, g on the right-hand side of Equation (3.1). We use the Gaussian quadrature method to integrate them more accurately. Since they are not evaluated by exact integration for the Crank-Nicolson scheme, we observe a quadrature error. Therefore, for the case using the Gaussian quadrature, we add zeros in (6.36) and write (6.31) as:

$$\begin{aligned}
\eta_{pert} &= \eta^u_{pert} + \eta^v_{pert} \\
&= \left(\rho^{G.Q}_u(\widetilde{u}_{kh}, \widetilde{v}_{kh})(\widetilde{z}_{1,kh}) - \rho^{trapz}_u(\widetilde{u}_{kh}, \widetilde{v}_{kh})(\widetilde{z}_{1,kh})\right) \\
&\quad + \left(\rho^{G.Q}_v(\widetilde{u}_{kh}, \widetilde{v}_{kh})(\widetilde{z}_{2,kh}) - \rho^{trapz}_v(\widetilde{u}_{kh}, \widetilde{v}_{kh})(\widetilde{z}_{2,kh})\right) \\
&\quad + \rho^{trapz}_u(\widetilde{u}_{kh}, \widetilde{v}_{kh})(\widetilde{z}_{1,kh}) + \rho^{trapz}_v(\widetilde{u}_{kh}, \widetilde{v}_{kh})(\widetilde{z}_{2,kh})
\end{aligned}$$

We use the notations in (6.38) and (6.40), and write as:

$$\begin{aligned}\eta_{pert} &= \eta^u_{quad} + \eta^v_{quad} + \eta^u_{split} + \eta^v_{split} \\ &=: \eta_{quad} + \eta_{split}.\end{aligned}$$

Finally, we achieve the separation of the error in (6.37),

6.6 Refinement Algorithm

In this section, we present the adaptive mesh refinement algorithm for space-time adaptivity based on the a posteriori error estimates introduced in the previous sections. We want to estimate the error functional $J(u,v) - J(u_{kh}, v_{kh})$ in terms of error estimators such that

$$J(u,v) - J(u_{kh}, v_{kh}) = |\eta^u_k + \eta^v_k + \eta^u_h + \eta^v_k + \eta_{pert}| < TOL, \tag{6.42}$$

In order to bring the total error under the tolerance TOL as shown above, we ensure that each estimator is under TOL:

$$\eta^u_k < TOL, \quad \eta^v_k < TOL, \quad \eta^u_h < TOL, \quad \eta^v_k < TOL, \quad \eta_{pert} < TOL_i \tag{6.43}$$

where TOL is the given accuracy for the discretization error and TOL_i for the perturbation error. Usually they are in the same order, unless specified for special cases. For the simplicity, we write the sum of estimators of two sub-parts as $\eta := \eta^{u+v}$.

The goal of the algorithm is to find a combination of four discretizations that is the coarsest possible through refining the discretizations separately and in the equilibrating reduction, until each derived estimator reaches the desired accuracy. The algorithm avoids unnecessary refinement of the discretization by assessing for each component and thus minimizes the computational cost. In order to obtain the optimal combination of the four discretizations on each refinement cycle, we must use the precise quantitative assessment of the error estimations derived in the previous section.

To this end, we introduce equilibrium constants κ_1 and κ_2 (see Line 14 and Line 7 in Algorithm 4.) Based on the mesh refinement algorithm by Goll, Rannacher, and Wollner [35], Schmich and Vexler [64], and Besier and Rannacher [13], choosing optimal $\kappa_i, i = 1, 2$ is done through a trial-and-error process. If κ_i is too small, then the refinement process slows down because the algorithm refines only one of the temporal or spatial discretization, even if the error estimators of the temporal and spatial discretizations are very close. On the other hand, if κ_i is too big, it refines

both temporal and spatial discretizations, even if the dominating error is from only one discretization.

Therefore, we develop an algorithm that prevents such drawbacks. Using the separated error estimates, the algorithm checks whether a temporal or spatial estimator of each sub-part has reached the desired accuracy before refining the discretization. For instance, if κ_i was too big, it would fall into the case to refine both discretizations in time and space. The algorithm goes through each estimator and refines only those that generate a discretization error estimate that is greater than the given tolerance. It then proceeds as described in Algorithm 4. Since we want to maintain the equilibrating reduction of the temporal and spatial discretization error, we use equilibration constants $\kappa_1 = 4$ and $\kappa_2 = 2$. These constants reflect the convergence rate of space and time discretizations for the implicit Euler method, and $\kappa_1 = 4$ and $\kappa_2 = 4$ for the Crank-Nicolson method.

As explained in the beginning of this chapter, another aspect that is refined in a balanced manner is between the two problems. Within the equilibrium between the error contributions from the temporal and spatial discretizations, we balance the error estimates for each sub-part: balance η_k^u and η_k^v in the temporal discretization, and balance η_h^u and η_h^v in the spatial discretization. This helps to avoid discretizations that are overly refined, as over-refinement results in extra computational cost or it remains too coarse, which might lead to the divergence of the algorithm.

Although the solutions of the system are solved in a split manner, they remain coupled within the system. Therefore, we must be very careful in choosing the discretization to maintain the accuracy of the solutions. For example, solving the parabolic problem on a very fine mesh does not guarantee convergence to the simultaneous solution or the convergence of the algorithm, if the error of the coupling term from the elliptic problem is too large. We have observed that a ratio that is too large between time step length of two temporal discretizations causes divergence. Therefore, the algorithm is designed to give the optimal combination of discretizations with the least computational cost, while maintaining the convergence and the error estimators under a given tolerance. See Line 16 of Algorithm 4, where divergence due to the splitting error is checked and thereby the temporal discretization of the elliptic problem is refined to reduce the ratio. The refinement cycle stops when all error contributions reach a desired accuracy. The diagram 6.3 shows the flow chart of the algorithm.

Remark 6.3. The initial discretization can be coarse as long as we obtain the convergence of the algorithm. In a case where an initial combination of discretizations does not give a converging iteration, one can apply the damped Crank-Nicolson, as explained in Section 4.4

Algorithm 4 Adaptive refinement algorithm

procedure
  Choose an initial space and time discretizations
  Set $n = 0$.
  repeat
    Calculate the primal and dual solutions following Algorithm 3
    Evaluate a posteriori error estimators η_k and η_h
    if $|\eta_h| > \kappa_2|\eta_k|$ **then**
      if $|\eta_h^u| > TOL$ **then**
        Adapt the spatial discretization of u
      end if
      if $|\eta_h^v| > TOL$ **then**
        Adapt the spatial discretization of v
      end if
    else if $|\eta_k| > \kappa_1|\eta_h|$ **then**
      if $|\eta_{pert}| > TOL_i$ **then**
        Adapt the temporal discretization of v
      else
        if $|\eta_k^u| > TOL$ **then**
          Adapt the temporal discretization of u
        end if
        if $|\eta_k^v| > TOL$ **then**
          Adapt the temporal discretization of v
        end if
      end if
    else
      if $|\eta_k^u| > TOL$ **then**
        Adapt the temporal discretization of u
      end if
      if $|\eta_k^v| > TOL$ **then**
        Adapt the temporal discretization of v
      end if
      if $|\eta_h^u| > TOL$ **then**
        Adapt the spatial discretization of u
      end if
      if $|\eta_h^v| > TOL$ **then**
        Adapt the spatial discretization of v
      end if
    end if
    Increase n.
  until there is no more refinement
end procedure

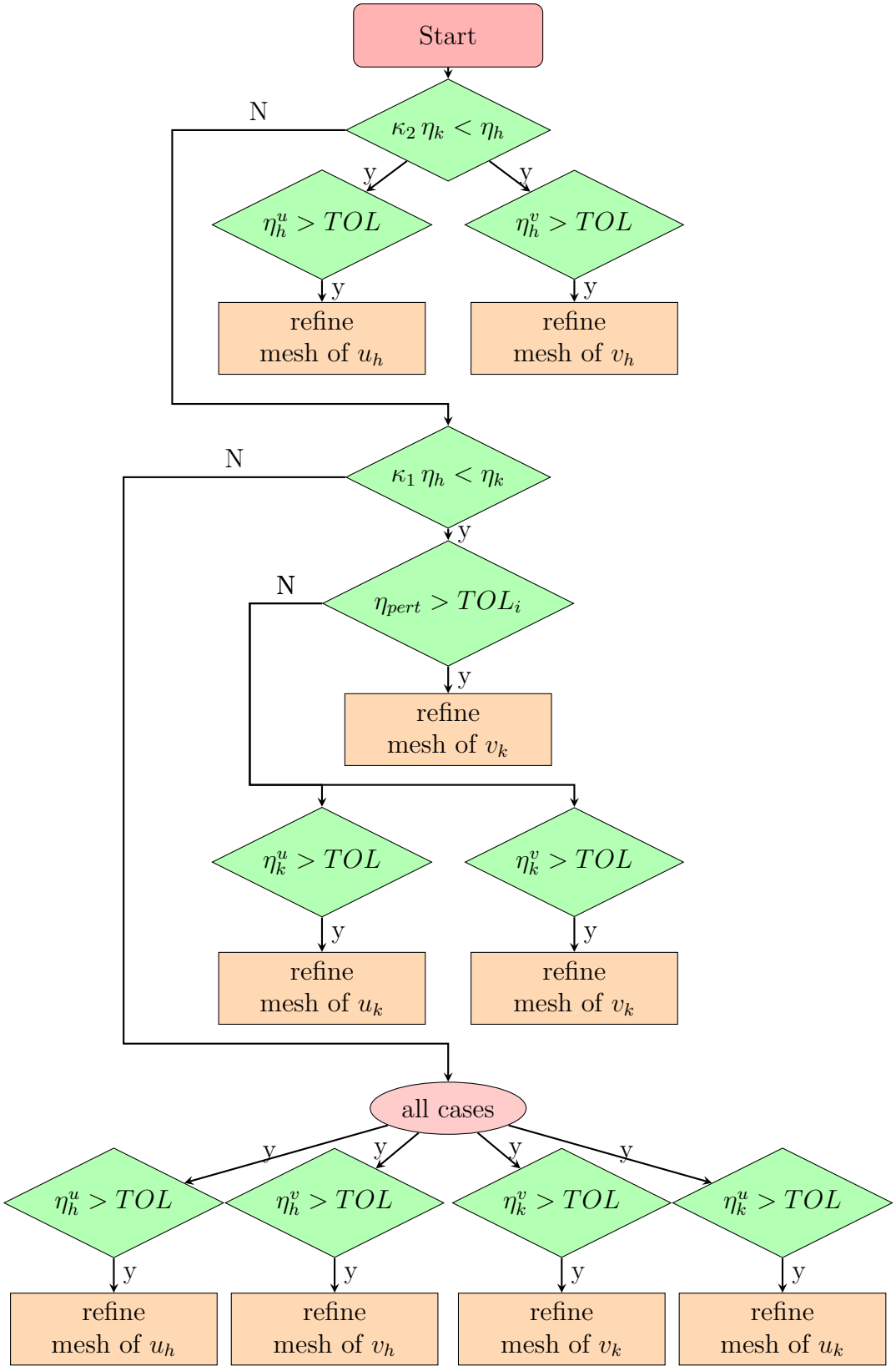

Figure 6.3. Flowchart for the iterative algorithm using multirate time stepping for the coupled system.

7 Numerical Results

In this chapter, we apply the adaptive mesh refinement algorithm and a posteriori error estimates developed in Chapter 6. We present the numerical results achieved by applying the adaptive algorithm in the coupled parabolic/elliptic system. We show the good quantitative assessment of the temporal and spatial discretization error estimators and the splitting error estimator that are validated by measuring their overestimation. First, we apply some constraints, such as fixing the spatial discretizations or fixing the ratio of time step lengths of the temporal discretizations. This helps us to see more clearly the independent behavior of discretization error estimators. Then, we present the tables and the graphs for the fully adaptive algorithm (no constraint). The errors computed with respect to the different functionals are compared.

To this end, we recall the model of the coupled parabolic/elliptic system:
Find u, v such that

$$\begin{aligned} \frac{\partial u(x,t)}{\partial t} - \Delta u(x,t) - \Delta v(x,t) &= f \quad \text{in } I \times \Omega\,, \\ -\Delta v(x,t) + v(x,t) - u(x,t) &= g \quad \text{in } I \times \Omega\,, \\ u &= u_0 \quad \text{in } 0 \times \Omega\,, \\ u &= 0 \quad \text{on } I \times \partial\Omega\,. \end{aligned}$$

Let the force terms f, g be given in such a way that the exact solutions u, v are given by

$$\begin{aligned} u(x,t) &= \cos(t)\sin(x)\,, \\ v(x,t) &= \cos(t)\sin(x)\,. \end{aligned}$$

The functional can be chosen for the interest of the physical model. In this work, we use two functionals. The first one is the average norm value over time interval $I = [0, T]$:

$$J_t := ((u(x,t), u(x,t))_\Omega)_I = \int_I \int_\Omega u(x,t)^2 \, dx \, dt, \tag{7.1}$$

where $\Omega = [0, \pi]$. This functional shows the chemical process on the cathode over time. Another functional is the norm value at the end-time, $t = T$:

$$J_T := (u(x,T), u(x,T))_\Omega. \tag{7.2}$$

This goal functional is focused on the status of the ion concentration after the process reaches at the end of the time interval. Note that these functionals do not involve the electric potential value. The following results in this chapter are for the case of cG(1)cG(1) discretization in one-dimensional space.

7.1 Numerical Results of the Error Estimators

We present the numerical justification for the separation of the total discretization error into a temporal and spatial contribution for both components of the system, u, v, and also the independent behavior of their error estimators.
Here, and in the rest of the chapter, n_h denotes the number of cells of spatial discretization while n_k denotes the number of subintervals in time. In the following tables, there are two columns for the perturbation error indicated as the column of $\eta_{pert}^{G.Q}$ and η_{pert}^{trapz}. We have seen that η_{pert}^{trapz} measures the perturbation error due to the splitting method. Thus, by subtracting η_{pert}^{trapz} from $\eta_{pert}^{G.Q}$, we obtain the estimate of the quadrature error. In this section, we used the Gaussian quadrature integration method with two points ($n = 2$). We observe that it gives the same quadratic convergence as for the Crank-Nicolson method. The last column show the *effectivity index*

$$I_{eff} := \left| \frac{\eta_h + \eta_k + \eta_{pert}}{J(e)} \right|,$$

where

$$J(e) := J(w - w_{kh}) = J(w) - J(w_{kh}), \tag{7.4}$$

which holds true for those linear functionals we choose to use. This index represents the degree of overestimation of in the resulting error estimators. Desirably, the effective index should to be close to one, which shows a very good error estimation. The successive rows in the tables are the uniform-refinement cycles, as clearly notable by the doubling of the number of cells.

First, we set a constraint by fixing the spatial discretizations in order to focus solely on the temporal discretization error estimates. Thus, in Table 7.1−Table 7.4, the spatial discretization is fixed such that its error estimate remains under the tolerance $TOL = 10^{-5}$. Also, both the parabolic and the elliptic problems are solved on the same temporal discretization on each cycle.

Table 7.1. For over-time functional J_t: Error estimates where the parabolic and elliptic equations are solved on a same discretization and for the cG(1)cG(1) discretization.

J_t, Ratio=1, $n_h = 256$								
n_k	η_h^{u+v}	η_k^u	η_k^v	η_k^{u+v}	$\eta_{pert}^{G.Q}$	η_{pert}^{trapz}	$J(e)$	I_{eff}
16	3.37e-05	8.75e-03	9.91e-05	8.85e-03	1.04e-02	-2.54e-09	1.57e-02	1.22
32	3.22e-05	2.14e-03	-1.85e-05	2.12e-03	2.70e-03	-6.94e-09	3.06e-03	1.58
64	3.13e-05	5.23e-04	-4.27e-06	5.19e-04	6.86e-04	-8.15e-09	5.75e-04	2.15
128	3.07e-05	1.29e-04	-6.57e-07	1.28e-04	1.73e-04	-2.20e-08	1.46e-04	2.27

Table 7.2. J_t: Error estimates where the parabolic equation is solved on a twice finer temporal discretization than for the elliptic equation.

J_t, Ratio=2, $n_h = 256$									
n_k^u	n_k^v	η_h^{u+v}	η_k^u	η_k^v	η_k^{u+v}	$\eta_{pert}^{G.Q}$	η_{pert}^{trapz}	$J(e)$	I_{eff}
32	16	3.17e-05	6.60e-04	3.68e-04	1.03e-03	1.13e-03	-2.07e-09	2.40e-03	0.91
64	32	3.10e-05	1.90e-04	-1.37e-06	1.88e-04	2.48e-04	-7.78e-09	-1.97e-04	2.38
128	64	3.06e-05	4.79e-05	-3.19e-06	4.47e-05	5.77e-05	-1.42e-08	-2.24e-04	0.60
256	128	3.04e-05	1.19e-05	-5.89e-07	1.13e-05	1.39e-05	-5.37e-08	-5.09e-05	1.09

Table 7.3. For end-time functional J_T: Error estimates where the parabolic and elliptic equations are solved on a same discretization and for the cG(1)cG(1) discretization.

J_T, Ratio=1, $n_h = 256$								
n_k	η_h^{u+v}	η_k^u	η_k^v	η_k^{u+v}	$\eta_{pert}^{G.Q}$	η_{pert}^{trapz}	$J(e)$	I_{eff}
16	1.71e-05	-8.34e-03	1.24e-01	1.16e-01	1.27e-02	-3.74e-09	1.22e-01	1.05
32	2.30e-05	-1.96e-03	3.15e-02	2.95e-02	2.86e-03	-7.46e-09	3.13e-02	1.04
64	2.54e-05	-4.67e-04	7.91e-03	7.44e-03	6.76e-04	-3.17e-09	7.91e-03	1.03
128	2.65e-05	-1.14e-04	1.98e-03	1.87e-03	1.64e-04	-2.00e-08	2.03e-03	1.02

The results with the goal functional over time J_t that is defined in Equation (7.1) are shown in Table 7.1. The first column for the spatial error estimator η_h^{u+v} shows the independent behavior; the spatial error estimator remains same as the temporal discretization is refined. By comparing the columns η_k^u and η_k^v, it is clear that the total temporal discretization error η_k^{u+v} is dominated by the temporal discretization error of the parabolic equation. The developed algorithm uses this information to avoid unnecessary refinement of the discretization of the elliptic equation to minimize the computational cost. This justifies the separation of each discretization error into the contribution of the sub-parts.
Moreover, we observe that for temporal discretization I_{eff} close to one, which implies that the error estimates are good. Looking at Table 7.2 where the set-up is as same as in Table 7.1, except that the additional constraint is applied. The two equations are solved on the discretizations such that the temporal discretization of the parabolic equation is twice finer than of the elliptic equation. Simply, we say it as $ratio = 2$, which is the ratio between the time step length of the temporal discretization of the parabolic equation and of the elliptic equation. We observe similar results in Table 7.1 and the good I_{eff} that converges to one.
The results in Table 7.3 and Table 7.4 are for the end-time functional J_T defined in Equation (7.2). Unlike the case of J_t, the error estimates of the elliptic equation dominates the total temporal discretization error. In both cases, we observe the very good quantitative estimation of the discretization error $I_{eff} \approx 1$.

Table 7.4. J_T: Error estimates where the parabolic equation is solved on a twice finer temporal discretization than for the elliptic equation.

J_T, Ratio=2, $n_h = 256$									
n_k^u	n_k^v	η_h^{u+v}	η_k^u	η_k^v	η_k^{u+v}	$\eta_{pert}^{G.Q}$	η_{pert}^{trapz}	$J(e)$	I_{eff}
32	16	2.02e-05	-2.91e-03	1.20e-01	1.17e-01	1.67e-03	2.18e-09	1.03e-01	1.15
64	32	2.45e-05	-7.47e-04	3.05e-02	2.97e-02	3.06e-04	-5.56e-10	2.65e-02	1.13
128	64	2.62e-05	-1.86e-04	7.66e-03	7.47e-03	6.27e-05	2.94e-10	6.72e-03	1.13
256	128	2.69e-05	-4.63e-05	1.92e-03	1.87e-03	1.39e-05	-2.99e-08	1.73e-03	1.11

7.2 Comparison with Different Goal Functionals

We have validated the discretization error estimators by the effectivity index and their independence under the constraints in the previous section. Now we are ready

to present the case with no constraint; all four discretizations in time and space for both parabolic and elliptic equations are independently refined until their error estimators are under the tolerance $TOL = 10^{-5}$.

Consider Table 7.5 for the case with J_t. We can choose the initial discretizations as coarse as we observe the convergence within the algorithm. In this case, we choose each discretization with 16 elements. Then the algorithm balances the error estimators of the four discretization errors during the refinement process. The effectivity index I_{eff} remains close to one in the beginning, then, as the ratio between the discretizations increases, I_{eff} decreases. We observe that the elliptic equation does not required as fine discretizations in space and time as the parabolic equation. After 12 successive refinements, all the error estimators reaches under the tolerance, and we terminate the refinement process.

One of the particular behaviors we must note is at the tenth cycle, where the total temporal discretization error and the perturbation error estimator are explored. Especially, the splitting error estimate η_{pert}^{trapz} is increased by 10^7. This shows that the perturbation error is dominated by the splitting error, and we then know that this error comes from someplace else, but it occurs due to the ratio of the time step lengths of two temporal discretizations that are too far apart. This divergence behavior is fixed by refining only the temporal discretization of the elliptic equation, as seen in the eleventh cycle. This is the justification for the separation of the perturbation error into the quadrature and splitting error estimates. It is easier to see the overall pattern of the refinement cycles and the decreasing pattern of each error in the plots in Figure 7.1 and Figure 7.2, where the error estimators in Table 7.5 and Table 7.6 are plotted over the refinement cycles.

Here, we use the following labels:

- "est error sp u": the spatial discretization error for the parabolic equation, η_h^u
- "est error sp v": the spatial discretization error for the elliptic equation, η_h^v
- "est error t u": the temporal discretization error for the parabolic equation, η_k^u
- "est error t v": the temporal discretization error for the elliptic equation, η_k^v
- "est error tol": the sum of perturbation error for the parabolic and elliptic equations, $\eta_{pert}^{G.Q}$

Figure 7.1 shows the refinement sequence for the equations whose functional is J_t. The spatial discretization errors for both equations are decreasing in parallel, thus both discretizations of the sub-parts are refined until the end of the cycle. However, for the discretization errors in time, it is clearly shown in the figure that η_k^v is much smaller than η_k^u, and $\eta_k^v < TOL$ after four refinement cycles, while η_k^u needs eleven

cycles. Thus, the temporal discretization of the elliptic equation is able to remain coarser than the temporal discretization of the parabolic equation.

The perturbation error (indicated by a black dashed line on the right) represents the divergence of the splitting method. We refine only the temporal discretization for the elliptic equation. Then we observe that the explosion of the error estimates vanishes, and we gain back the convergence behavior on the next cycle. Therefore, the role of the perturbation error estimate and the separation into the quadrature and the splitting error is crucial to know how to effectively fix the divergence behavior by knowing precisely where the abnormal increase of the error is coming from.

When the functional J_T is taken, the discretizations for both equations are refined together, and we do not see much of the benefit from the adaptive algorithm. However, instead of running with all the coefficients as $\alpha_i = 1$, $i = 1, \cdots, 5$, which we arbitrarily set to simulate initially, we run with the coefficients $\alpha_2 = 0.1$ and $\alpha_3 = 0.1$. These values are closer to the ones from the physical model. The result of the adaptive refinement for the functional J_T is found in Table 7.7 and Figure 7.3, where the values from the table is plotted. The temporal discretization of the elliptic equation will not be refined after the eighth cycle, since its error estimator already reached below the tolerance $TOL = 10^{-5}$. Thus, the efficiency of the adaptive method is emphasized in the model with values that are close to the ones from the physical model.

Adaptive refinement in space and in time, J_t													
n_h^u	n_h^v	n_k^u	n_k^v	η_h^u	η_h^v	η_h^{u+v}	η_k^u	η_k^v	η_k^{u+v}	$\eta_{pert}^{G.Q}$	η_{pert}^{trapz}	$J(e)$	I_{eff}
16	16	16	16	1.17e-02	-3.06e-03	8.59e-03	9.07e-03	-2.75e-04	8.79e-03	1.03e-02	3.23e-10	2.27e-02	1.22
32	32	16	16	2.93e-03	-7.68e-04	2.16e-03	9.11e-03	-2.75e-04	8.84e-03	1.03e-02	6.20e-10	1.22e-02	1.75
32	32	32	32	2.77e-03	-7.10e-04	2.06e-03	2.14e-03	-1.85e-05	2.12e-03	2.69e-03	1.07e-09	6.41e-03	1.07
64	64	32	32	6.93e-04	-1.78e-04	5.16e-04	2.16e-03	-4.22e-05	2.12e-03	2.70e-03	1.89e-10	2.40e-03	2.23
64	64	64	64	6.70e-04	-1.70e-04	5.00e-04	5.23e-04	-4.27e-06	5.19e-04	6.86e-04	-6.04e-09	1.36e-03	1.25
128	128	64	64	1.67e-04	-4.24e-05	1.25e-04	5.25e-04	-5.75e-06	5.19e-04	6.86e-04	-7.35e-09	5.12e-04	2.60
128	128	128	64	1.64e-04	-4.18e-05	1.23e-04	4.86e-05	-5.57e-06	4.30e-05	5.77e-05	-1.44e-08	-2.89e-04	0.77
256	256	256	64	4.06e-05	-1.04e-05	3.03e-05	-2.84e-05	-5.53e-06	-3.39e-05	-1.01e-04	-3.33e-08	-6.42e-04	0.16
512	512	512	64	1.01e-05	-2.58e-06	7.53e-06	-2.73e-05	-5.51e-06	-3.28e-05	-1.41e-04	-3.83e-08	-7.30e-04	0.23
512	512	1024	64	1.03e-05	-2.26e-06	8.04e-06	1.41e-03	5.01e-03	6.42e-03	1.82e-01	1.82e-01	-3.65e+14	0.00
512	512	1024	128	1.01e-05	-2.55e-06	7.53e-06	-6.82e-06	-5.68e-07	-7.39e-06	-3.60e-05	1.04e-07	-1.51e-04	0.24
1024	512	1024	128	2.52e-06	-4.99e-20	2.52e-06	-6.81e-06	-8.07e-07	-7.62e-06	-3.97e-05	-3.60e-06	-1.84e-04	0.24

Table 7.5. Adaptive refinement on the spatial and temporal discretizations for J_t and the tolerance $TOL = 10^{-5}$

Adaptive refinement in space and in time, J_T													
n_h^u	n_h^v	n_k^u	n_k^v	η_h^u	η_h^v	η_h^{u+v}	η_k^u	η_k^v	η_k^{u+v}	$\eta_{pert}^{G.Q}$	η_{pert}^{trapz}	$J(e)$	I_{eff}
8	8	16	16	3.17e-02	-1.47e-02	1.70e-02	-8.36e-03	1.25e-01	1.16e-01	1.26e-02	9.74e-10	1.82e-01	0.804
8	8	32	32	3.43e-02	-1.14e-02	2.29e-02	-1.96e-03	3.17e-02	2.97e-02	2.84e-03	1.23e-09	9.27e-02	0.598
16	16	32	32	8.72e-03	-2.77e-03	5.95e-03	-1.99e-03	7.84e-03	5.86e-03	2.85e-03	2.46e-10	2.43e-02	0.604
32	32	32	32	2.19e-03	-6.94e-04	1.50e-03	-1.99e-03	7.83e-03	5.85e-03	2.86e-03	-5.11e-10	1.26e-02	0.808
64	64	32	32	5.48e-04	-1.74e-04	3.74e-04	-1.99e-03	7.83e-03	5.85e-03	2.86e-03	-1.84e-09	9.70e-03	0.936
64	64	64	64	5.68e-04	-1.62e-04	4.06e-04	-4.67e-04	7.91e-03	7.44e-03	6.75e-04	-5.01e-09	8.82e-03	0.966
64	64	128	128	5.78e-04	-1.54e-04	4.24e-04	-1.14e-04	1.98e-03	1.87e-03	1.64e-04	-8.03e-09	2.94e-03	0.835
64	64	256	256	5.83e-04	-1.50e-04	4.32e-04	-2.80e-05	4.95e-04	4.67e-04	4.04e-05	-1.26e-09	1.47e-03	0.641
128	128	256	256	1.46e-04	-3.75e-05	1.08e-04	-2.80e-05	1.24e-04	9.57e-05	4.04e-05	-1.21e-09	3.81e-04	0.642
256	256	256	256	3.64e-05	-9.38e-06	2.70e-05	-2.80e-05	1.24e-04	9.57e-05	4.04e-05	-1.24e-09	1.98e-04	0.825
512	256	256	256	9.11e-06	-4.01e-19	9.11e-06	-2.80e-05	1.22e-04	9.36e-05	2.68e-05	-1.36e-05	1.62e-04	0.801
512	256	512	512	9.14e-06	3.09e-20	9.14e-06	-6.94e-06	1.18e-04	1.11e-04	-3.66e-06	-1.37e-05	1.42e-04	0.824
512	256	1024	1024	9.16e-06	6.85e-19	9.16e-06	-1.73e-06	1.91e-05	1.74e-05	-1.12e-05	-1.37e-05	4.48e-05	0.341
512	256	1024	1024	9.16e-06	6.85e-19	9.16e-06	-1.73e-06	-4.14e-06	-5.87e-06	-1.12e-05	-1.37e-05	2.26e-05	0.351

Table 7.6. Adaptive refinement on spatial and temporal discretizations for J_T and the tolerance $TOL = 10^{-5}$

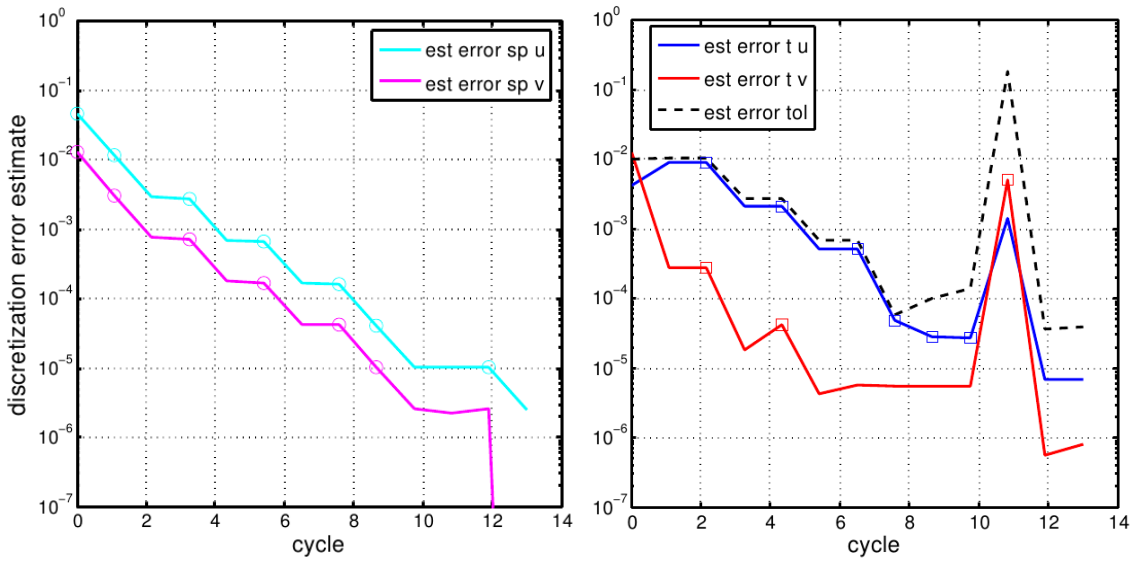

Figure 7.1. Show the adaptive algorithm mesh refinement for the functional the norm value over time J_t. (left): The spatial discretization error estimate for each cycle and circles indicates that the mesh is refined in next cycle. (right): The temporal discretization error estimate and squares indicate the refinement. The black dashed line indicates the splitting error estimate.

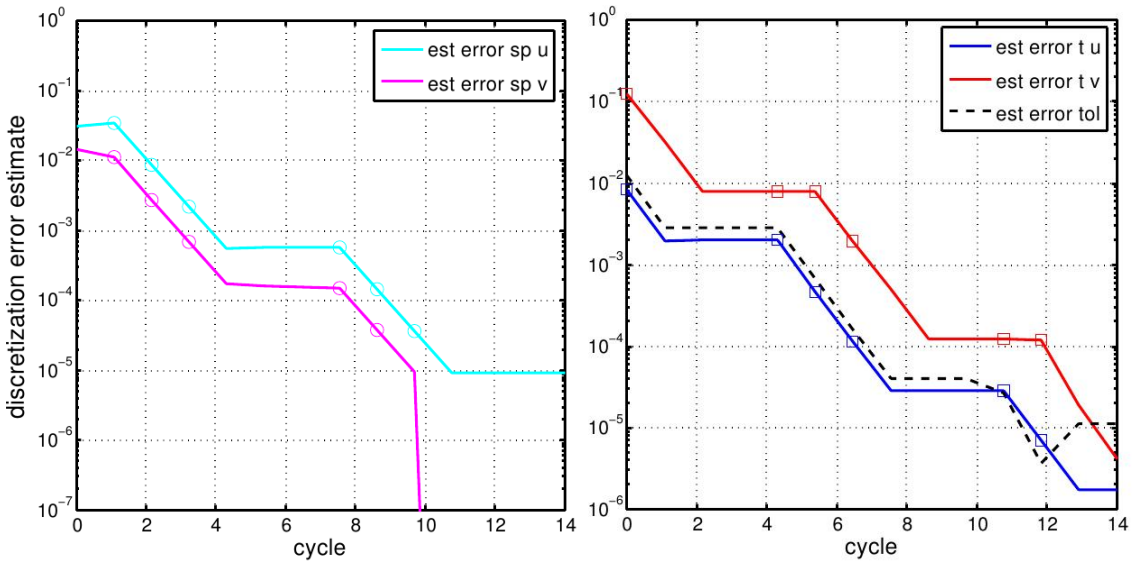

Figure 7.2. Show the adaptive algorithm mesh refinement for the functional the norm value at the end-time J_T. Same as in Figure 7.1 for indicators.

Adaptive refinement in space and in time, J_T, $\alpha_2 = 0.1$ and $\alpha_3 = 0.1$													
n_h^u	n_h^v	n_k^u	n_k^v	η_h^u	η_h^v	η_h^{u+v}	η_k^u	η_k^v	η_k^{u+v}	$\eta_{pert}^{G.Q}$	η_{pert}^{trapz}	$J(e)$	I_{eff}
8	8	16	16	2.30e-03	-1.40e-03	9.04e-04	-5.58e-03	1.25e-02	6.92e-03	1.67e-02	1.99e-10	1.62e-01	0.152
8	8	32	32	2.22e-03	-8.86e-04	1.33e-03	-3.36e-03	3.17e-03	-1.93e-04	4.13e-03	-2.63e-09	5.80e-02	0.091
16	16	32	32	5.23e-04	-2.11e-04	3.12e-04	-3.31e-03	7.81e-04	-2.53e-03	4.14e-03	-2.58e-09	1.91e-02	0.101
16	16	64	64	5.08e-04	-1.68e-04	3.41e-04	-1.81e-03	7.92e-04	-1.02e-03	1.03e-03	7.90e-11	1.46e-02	0.024
32	32	128	64	1.23e-04	-3.63e-05	8.67e-05	-9.42e-04	1.72e-04	-7.71e-04	2.53e-04	-1.13e-09	3.17e-03	0.136
32	32	256	128	1.22e-04	-3.33e-05	8.87e-05	-4.81e-04	1.92e-04	-2.89e-04	6.28e-05	-5.63e-08	3.26e-03	0.042
64	64	512	256	3.02e-05	-7.91e-06	2.23e-05	-2.42e-04	4.80e-05	-1.94e-04	1.57e-05	-6.72e-09	8.15e-04	0.192
64	64	1024	512	3.02e-05	-7.71e-06	2.25e-05	-1.22e-04	1.20e-05	-1.10e-04	3.92e-06	3.40e-09	4.66e-04	0.179
64	64	2048	1024	3.01e-05	-7.61e-06	2.25e-05	-6.10e-05	3.00e-06	-5.80e-05	9.96e-07	1.66e-08	3.78e-04	0.091

Table 7.7. Adaptive refinement on spatial and temporal discretizations for J_T and the tolerance $TOL = 10^{-5}$ with $\alpha_2 = 0.1$ and $\alpha_3 = 0.1$

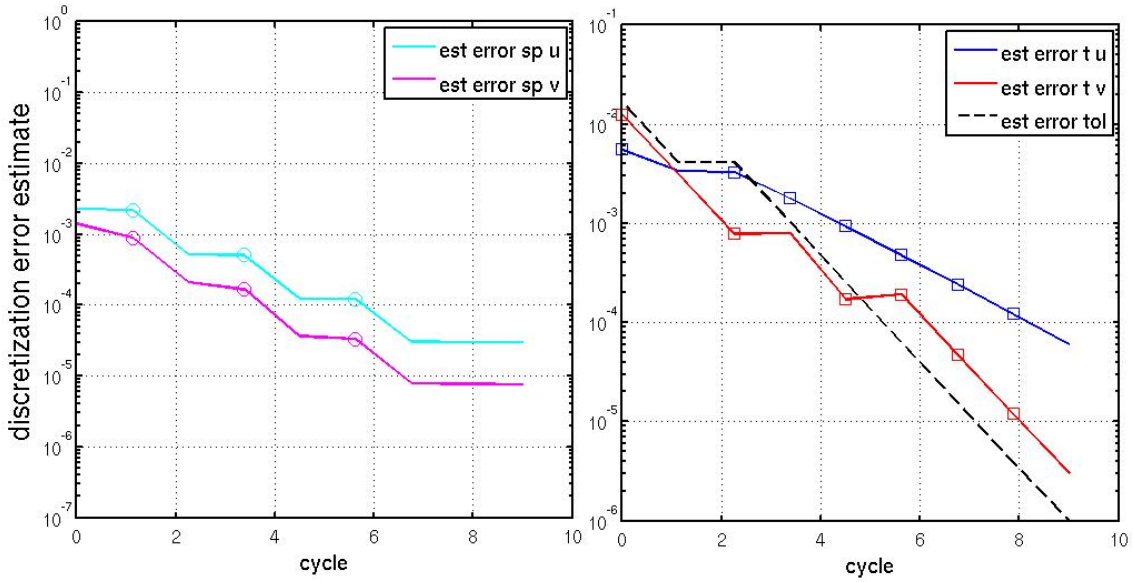

Figure 7.3. Show the adaptive algorithm mesh refinement for the functional the norm value at the end-time J_T with the coefficients $\alpha_2 = 0.1$ and $\alpha_3 = 0.1$. Same as in Figure 7.2 for indicators.

8 Conclusion and Outlook

This thesis is devoted to the development of an efficient numerical adaptive mesh refinement algorithm for solving the coupled parabolic/elliptic system. This algorithm uses finite element discretizations in time and space. Based on the discretizations, we derived a posteriori error estimates by means of the Dual Weighted Residual method. These estimates determine the discretization errors measured in some quantity of interest. First, we separated the discretization errors in time and space. This separation enables the independent refinement of each discretization. We then used this information for the proposed algorithm to refine the temporal and spatial discretizations on each cycle until their errors reach the desired accuracy. This independent refinement is realized in such a way that the error contributions of the temporal and spatial discretizations are balanced. On each cycle, the accuracy of the estimates are validated by the effective index.

By the operator splitting method called the iterative (sequential) method, the fully-discretized (in time and space) system is decoupled into two sub-parts: parabolic and elliptic problems. This decoupled sequential approach gives us the freedom to use the standard solvers and may save some computational cost. We chose to solve two problems by the multirate iterative solving method, i.e., solve two equations in different time scales. Due to the coupling terms, in addition to balancing the error contributions between the temporal and spatial discretizations, we also balanced the discretization error contributions from the two sub-parts. Thus, an a posteriori perturbation error estimate was derived, which was further separated into the splitting error and the quadrature error caused by using an inexact numerical integration method.
The perturbation error estimate was also controlled within the developed adaptive algorithm and was balanced with the discretization error estimates. The perturbation error estimate was used to find the optimal ratio between discretizations of the two sub-parts for the least computational cost, while maintaining the convergence of the iterations within the developed algorithm.

Finally, the developed numerical adaptive algorithm was applied for the simulation of a simplified 1D cathode model. In our simulation, the parabolic part of the system represents the concentration distribution of ions, and the elliptic part represents the electrical potential within the cathode. We observed the savings in the computational

time: we found the least required degrees of freedom for both equations to obtain the desired accuracy.
This least degrees of freedom for each equation are further enhanced by the multirate method. For the electric potential equation living in the faster time scale than the diffusion equation, we observe as we expected that the number of the degrees of freedom for the elliptic equation was smaller than those in the parabolic equation to reach the same order of accuracy. This significantly saves the total computational cost since the elliptic equation is more expensive to solve due to its greater condition number, as explained in Section 5.1. This combination of the least degrees of freedoms is optimal in that it maintains the convergence of the coupling iteration with the least computational cost for solving the system while achieving the accuracy we wanted.

Possible Future Work

Currently, we are working on proving the contraction for the fixed-point iteration of the developed algorithm. Also, most importantly, this work should be extended in 2D or 3D to simulate the physical model realistically. In higher dimensional spaces, the computational cost saved by using the developed mesh refinement algorithm is greater than in 1D. Moreover, instead of the constant coefficients, they can depend on the solutions. The Robin boundary condition from the original model can be used for a 2D or 3D model to consider the Triple Phase Boundary, where the electrochemical conversion occurs, or at the boundary where the chemical reaction with oxygen occurs. Then, instead of uniform mesh refinement, an effective choice will be the local spatial mesh refinement via use of the cell-wise error indicators derived in Section 6.3. Lastly, the development of the algorithm can be applied to any coupled model. Particularly, the model can be modified for batteries that are similar to fuel cell models.

9 Acknowledgments

Although far from home, I was able to form a hugely supportive academic family with people I have come to respect and rely on. My deepest appreciation goes to my supervisor, Prof. Rolf Rannacher, for welcoming me to his group in Heidelberg with open arms and "open doors" for my Ph.D work and job opportunities. It was a great privilege for me to have him as my supervisor. He was continuously kind, patient and supportive of all the ideas I brought to his table, and I am honored to have had the experience working with him.

I would also like to express my heartfelt thanks to my supervisor, Dr. Thomas Carraro for our countless discussions and his many helpful suggestions for my thesis. I would not have come this far without his guidance in Numeric and dealII in addition to his time and kind concern. Whenever I faced a problem, he always encouraged me with warm advice. He was a wonderfully helpful motivator in difficult times.

In addition to my advisers, I am indebted to Prof. Francesco Ciucci, who brought me to Germany with the European Union Marie Curie Reintegration Grant funding. Without him, I would not have explored academics and life in Germany. I thank him especially for suggesting I apply my mathematical skills to the study of clean energy.

I wish to thank Frau Fitzer and the entire Numerical Analysis Group of Heidelberg University. I am blessed to have such sincerely kind and great mathematicians as my colleagues. I am proud to be a member of this group, and had a great time getting to know each of its members. Sincere thanks to Felix Brinkmann, Simon Dörsam, Stefan Frei, Dr. Daniel Gerecht, Dr. Christian Goll, Dr. Adrian Hirn, Dr. Bärbel Janssen. Dr. Matthias Klinger, Dr. Matthias Maier, Vladislav Olkhovskiy, Victoria Ponce, Prof. Thomas Richter, Ina Schüssler, Florian Sonner, Judith Stein, Dr. Jevgeni Vihharev, Sven Wetterauer, and Prof. Thomas Wick for their many helpful ideas and discussions. Special thanks to Dr. Elfriede Friedmann for her warm support that came with the funding for modeling for ophthalmology during my last semester.

I gratefully acknowledge the European Union Marie Curie Grant funding I received during my doctoral studies. This grant helped me to pursue my dreams and find a world of support in a far-away place. I also gratefully acknowledge the Heidelberg

Graduate School of Mathematical and Computational Methods for the Science. As one of its members, I was given financial support for travel to attend conferences to present my work and receive the feedback, as well as to gain experience in research and connect with other great mathematicians during my doctoral research at the Faculty of Mathematics and Computer Science.

I thank all my friends in Germany and abroad, with whom I can share my joy, sadness and prayer.

I offer my love and gratitude to my father Jongan, my mother Haim, and my sister Bora, for their never-ending love and prayer. I also send my love to my grandmothers, who were and still are my life mentors and who still give me strength and light on my path. Finally, I wish to thank Gyeongsu for bearing with me and being there for me.

Most of all, I thank the Lord for his boundless love and endless blessing pouring into in my life.

Nomenclature

λ_D	Debye length
D_{eon}	Diffusivity of electrons
D_{ion}	Diffusivity of vacancies
H_0^1	Sobolev space of order 2 with homogeneous Dirichlet boundary condition
I	Open time interval $(0, T)$
I_m	Subinterval of time
I_{eff}	Effectivity index describing the quantitative behavior of the error estimators
$J(e)$	True error: $J(e) := J(w_{ex} - w_h)$
$J^{'}$	Quantity of interest (a linear and continuous functional)
$L^2(\Omega)$	Lebesgue space of measurable, square integrable functions
T	End time
T	Temperature in Chapter 2
T_h	Family of quasi-uniform meshes
V_{th}	Thermal voltage
X_k^r	Semi-discrete space contains the continuous piecewise polynomials degree up to r
$X_{kh}^{r,s}$	Space-time finite element space contains the continuous piecewise polynomials degree up to r
$[\cdot]$	Jump over boundary ∂K

Δ	$\frac{\partial^2}{\partial x_1^2} + \frac{\partial_2}{\partial x_2^2}$ Laplacian
$\Delta_{\tilde{x}}$	$\frac{\partial^2}{\partial \tilde{x}_1^2} + \frac{\partial_2}{\partial \tilde{x}_2^2}$ Dimensionless Laplacian
Γ_j	Boundaries of an element in mesh
Ω	Bounded computational domain
α_i	Positive constant coefficients
$\bar{I}$	Closed time interval $[0, T]$
$\bar{\phi}_{ion}$	Equilibrium value of electric potential
$\bar{c}_{ion}$	Equilibrium value of vacancy concentration
$\delta\phi_{ion}$	Perturbed value of electric potential
δc_{ion}	Perturbed value of vacancy concentration
ϵ_0	Local permittivity of the medium
η_h^u	Spatial error estimate of u
η_h^v	Spatial error estimate of v
η_h^w	Spatial discretization error indicator for w
η_h^{u+v}	Sum of spatial error estimates of u and v
η_k^u	Temporal error estimate of u
η_k^v	Temporal error estimate of v
η_k^w	Temporal discretization error indicator for w
η_k^{u+v}	Sum of temporal error estimates of u and v
$\eta_{\|K}$	Local discretization error indicator for a sampling cell $K \in T_h$
$\eta_{iter}^{G.Q}$	Sum of perturbation error estimates of u and v calculated by Gaussian Quadrature

η_{iter}^{trapz}	Sum of ieration error estimates of u and v calculated by Trapezolidal Rule
$\mathbf{K}$	Stiffness matrix $\mathbf{K}$
$\mathbf{M}$	Mass matrix $\mathbf{M}$
$\mathcal{L}$	Lagrangian function
∇	$(\frac{\partial}{\partial x_1}, \frac{\partial}{\partial x_2})$ Gradient
$\nabla_{\tilde{x}}$	$(\frac{\partial}{\partial \tilde{x}_1}, \frac{\partial}{\partial \tilde{x}_2})$ Dimensionless gradient
ϕ	Electric potential
τ	Characteristic timescale of diffusion
τ_{eon}	Characteristic timescale of electronic diffusion
τ_{ion}	Characteristic timescale of vacancy diffusion
$\mathbf{J}^{charge}$	Charge flux
$\mathbf{J}^{mass}$	Mass flux
$\tilde{\mu}$	Electrochemical potential
$\tilde{\mu}_i^*$	Normalized electrochemical potential
$\tilde{\phi}$	Dimensionless electric potential
$\widetilde{X}_k^r$	Semi-discrete space contains the discontinuous piecewise polynomials degree up to r
$\widetilde{X}_{kh}^{r,s}$	Space-time finite element space contains the discontinuous piecewise polynomials degree up to r
$a(\cdot,\cdot)$	Bilinear form $a : \bar{X} \to \mathbb{R}$
c_i	Carrier concentration
c_i^0	Reference value for carrier concentration

e	Elementary charge of an electron
eon	Electron
f	External force on u
g	External force on v
h_s	Area of an element in mesh
i	Charged species: electron or vacancy
ion	Oxygen vacancy
k_B	Boltzmann constant
k_m	Time step length between t_{m-1} and t_m
l_c	Characteristic length scale of the sample
m	time step index
n_h^u	Number of cells in space mesh of u
n_h^v	Number of cells in space mesh of v
n_k^u	Number of cells in time mesh of u
n_k^v	Number of cells in time mesh of v
t	Time
u	Oxygen ion concentration
v	Chemical potential
w^m	Value at the time step t_m
w_k	Solution of the semi-discretized problem
w_{kh}	Solution of the fully discretized problem
w_o	Initial value
x_i	(x_1, x_2) space coordinate

z_i	Integer charge of species i
DWR	Dual weighted residual
cG(r)	Time finite element discretization with continuous piecewise polynomials of degree s
cG(s)	Space finite element discretization with continuous piecewise polynomials of degree s
dG(r)	Time finite element discretization with discontinuous piecewise polynomials of degree s
id	Identity matrix

List of Tables

List of Figures

List of Algorithms

Bibliography

[1] R.A. Adams and J.J.F. Fournier. *Sobolev Spaces*. Pure and Applied Mathematics. Elsevier Science, 2003. ISBN 9780080541297. URL `https://books.google.fr/books?id=R5A65Koh-EoC`.

[2] Georgios Akrivis, Charalambos Makridakis, Ricardo, and H. Nochetto. A posteriori error estimates for the Crank– Nicolson method for parabolic equations. *Math. Comp*, pages 511–531.

[3] Tameem Almani, Ali H Dogru, Kundan Kumar, Gurpreet Singh, and Mary F Wheeler. Convergence of Multirate Iterative Coupling of Geomechanics with Flow in a Poroelastic Medium. *Saudi Aramco Journal of Technology, Spring*, 2016.

[4] Mario Arioli, Jörg Liesen, Agnieszka Miçdlar, and Zdeněk Strakoš. Interplay between discretization and algebraic computation in adaptive numerical solutionof elliptic PDE problems. *GAMM-Mitteilungen*, 36(1):102–129, 2013.

[5] F Armero and JC Simo. A new unconditionally stable fractional step method for non-linear coupled thermomechanical problems. *International Journal for numerical methods in Engineering*, 35(4):737–766, 1992.

[6] Francisco Armero. Formulation and finite element implementation of a multiplicative model of coupled poro-plasticity at finite strains under fully saturated conditions. *Computer methods in applied mechanics and engineering*, 171(3): 205–241, 1999.

[7] I. Babuška and J. E. Osborn. Finite Element-Galerkin Approximation of the Eigenvalues and Eigenvectors of Selfadjoint Problems. *Mathematics of Computation*, 52(186), 1989. ISSN 00255718. doi: 10.2307/2008468. URL `http://dx.doi.org/10.2307/2008468`.

[8] Ivo Babuška and Theofanis Strouboulis. *The finite element method and its reliability*. Oxford university press, 2001.

[9] Wolfgang Bangerth and Rolf Rannacher. *Adaptive finite element methods for differential equations*. Springer, 2003.

[10] Eberhard Bänsch. An adaptive finite-element strategy for the three-dimensional time-dependent Navier-Stokes equations. *Journal of Computational and Applied Mathematics*, 36(1):3–28, 1991.

[11] Roland Becker and Rolf Rannacher. An optimal control approach to a posteriori error estimation in finite element methods. *Acta Numerica*, 10:1–102, 5 2001. ISSN 1474-0508. doi: 10.1017/S0962492901000010. URL `http://journals.cambridge.org/article_S0962492901000010`.

[12] Roland Becker, Hartmut Kapp, and Rolf Rannacher. Adaptive finite element methods for optimal control of partial differential equations: Basic concept. *SIAM Journal on Control and Optimization*, 39(1):113–132, 2000.

[13] Michael Besier and Rolf Rannacher. Goal-oriented space–time adaptivity in the finite element galerkin method for the computation of nonstationary incompressible flow. *International Journal for Numerical Methods in Fluids*, 70(9): 1139–1166, 2012.

[14] Dietrich Braess. *Finite elements: Theory, fast solvers, and applications in solid mechanics*. Cambridge University Press, 2007.

[15] Susanne C. Brenner and L. Ridgway Scott. *The Mathematical Theory of Finite Element Methods*. Springer, 2nd edition, April 2002. ISBN 0387954511. URL `http://www.amazon.com/exec/obidos/redirect?tag=citeulike07-20&path=ASIN/0387954511`.

[16] John C Butcher. *Numerical methods for ordinary differential equations*. John Wiley & Sons, 2008.

[17] Haile SM Chueh WC1. Ceria as a thermochemical reaction medium for selectively generating syngas or methane from H(2)O and CO(2). *ChemSusChem*, 2(8): 735–739, Dec 2009. doi: 10.1002/cssc.200900138.

[18] Bernardo Cockburn, George E. Karniadakis, and Chi-Wang Shu. *The Development of Discontinuous Galerkin Methods*, pages 3–50. Springer Berlin Heidelberg, Berlin, Heidelberg, 2000. ISBN 978-3-642-59721-3. doi: 10.1007/978-3-642-59721-3_1. URL `http://dx.doi.org/10.1007/978-3-642-59721-3_1`.

[19] B. Cook. Introduction to fuel cells and hydrogen technology. *Engineering Science and Education Journal*, 11(6):205–216, Dec 2002. ISSN 0963-7346. doi: 10.1049/esej:20020601.

[20] Cox Peter M., Betts Richard A., Jones Chris D., Spall Steven A., and Totterdell Ian J. Acceleration of global warming due to carbon-cycle feedbacks in a coupled climate model. *Nature*, 408(6809):184–187, nov 2000. ISSN 0028-0836. doi: 10.1038/35041539. 10.1038/35041539.

[21] Rick H Dean, Xiuli Gai, Charles M Stone, Susan E Minkoff, et al. A comparison of techniques for coupling porous flow and geomechanics. *Spe Journal*, 11(01): 132–140, 2006.

[22] K. Eriksson and C. Johnson. Adaptive Finite Element Methods for Parabolic Problems V: Long-Time Integration. *SIAM Journal on Numerical Analysis*, 32 (6):1750–1763, 1995. ISSN 00361429. URL `http://www.jstor.org/stable/2158527`.

[23] Kenneth Eriksson and Claes Johnson. Adaptive Finite Element Methods for Parabolic Problems I: A Linear Model Problem. *SIAM Journal on Numerical Analysis*, 28(1):43–77, 1991. ISSN 00361429. URL `http://www.jstor.org/stable/2157933`.

[24] Kenneth Eriksson and Claes Johnson. Adaptive finite element methods for parabolic problems II: Optimal error estimates in L-infinite L2 and L-infinite L-infinite. *SIAM Journal on Numerical Analysis*, 32(3):706–740, 1995. ISSN 00361429. URL `http://www.jstor.org/stable/2158445`.

[25] Kenneth Eriksson and Claes Johnson. Adaptive finite element methods for parabolic problems IV: Nonlinear problems. *SIAM Journal on Numerical Analysis*, 32(6):1729–1749, 1995.

[26] Kenneth Eriksson, Don Estep, Peter Hansbo, and Claes Johnson. Introduction to Adaptive Methods for Differential Equations. *Acta Numerica*, 4:105–158, 1 1995. ISSN 1474-0508. doi: 10.1017/S0962492900002531. URL `http://journals.cambridge.org/article_S0962492900002531`.

[27] Kenneth Eriksson, Claes Johnson, and Stig Larsson. Adaptive Finite Element Methods For Parabolic Problems. VI. Analytic Semigroups. *SIAM J. Numer. Anal*, 28:43–77, 1998.

[28] Kenneth Eriksson, Claes Johnson, and Stig Larsson. Adaptive Finite Element Methods for Parabolic Problems VI: Analytic Semigroups. *SIAM J. Numer. Anal.*, 35(4):1315–1325, August 1998. ISSN 0036-1429. doi: 10.1137/S0036142996310216. URL `http://dx.doi.org/10.1137/S0036142996310216`.

[29] Alexandre Ern and Martin Vohralík. Adaptive Inexact Newton Methods with A Posteriori Stopping Criteria for Nonlinear Diffusion PDEs. *SIAM Journal on Scientific Computing*, 35(4):A1761–A1791, 2013. doi: 10.1137/120896918. URL `http://dx.doi.org/10.1137/120896918`.

[30] Steinar Evje and Kenneth Hvistendahl Karlsen. *Degenerate Convection-Diffusion Equations and Implicit Monotone Difference Schemes*, pages 285–294. Birkhäuser Basel, Basel, 1999. ISBN 978-3-0348-8720-5. doi: 10.1007/978-3-0348-8720-5_31. URL `http://dx.doi.org/10.1007/978-3-0348-8720-5_31`.

[31] Robert Eymard, Thierry Gallouït, Raphaèle Herbin, and Anthony Michel. Convergence of a finite volume scheme for nonlinear degenerate parabolic equations. *Numerische Mathematik*, 2002.

[32] M. Farooque and H.C. Maru. Fuel cells-the clean and efficient power generators. *Proceedings of the IEEE*, 89(12):1819–1829, Dec 2001. ISSN 0018-9219. doi: 10.1109/5.975917.

[33] JOANNE T Fredrich, JG Arguello, GL Deitrick, EP De Rouffignac, et al. Geomechanical modeling of reservoir compaction, surface subsidence, and casing damage at the Belridge diatomite field. *SPE Reservoir Evaluation & Engineering*, 3(04):348–359, 2000.

[34] Xiuli Gai, Shuyu Sun, Mary Fanett Wheeler, Hector Klie, et al. A Time-Stepping Scheme for Coupled Reservoir Flow and Geomechanics. In *SPE Annual Technical Conference and Exhibition*. Society of Petroleum Engineers, 2005.

[35] Christian Goll, Rolf Rannacher, and Winnifried Wollner. The damped Crank-Nicolson time-marching scheme for the adaptive solution of the Black–Scholes equation. *J. Comput. Finance (to appear)*, 2014.

[36] Thomas Grätsch and Klaus-Jürgen Bathe. A posteriori error estimation techniques in practical finite element analysis, 2005.

[37] P. Grisvard. *Elliptic Problems in Nonsmooth Domains*. CHAPMAN AND HALL /CRC MONOGRAPHS AND SURVEYS IN PURE AND APPLIED MATHEMATICS. John Wiley & Sons Australia, Limited, 1986. ISBN 9780470204849. URL `https://books.google.de/books?id=Rvy1PQAACAAJ`.

[38] J. Hoffman. Efficient computation of mean drag for the subcritical flow past a circular cylinder using general Galerkin G2. *International Journal for Numerical Methods in Fluids*, 59(11):1241–1258, 2009. ISSN 1097-0363. doi: 10.1002/fld.1865. URL `http://dx.doi.org/10.1002/fld.1865`.

[39] H. Holden. *Splitting Methods for Partial Differential Equations with Rough Solutions: Analysis and MATLAB Programs*. EMS series of lectures in mathematics. European Mathematical Society, 2010. ISBN 9783037190784. URL `https://books.google.de/books?id=wzobS67jfY4C`.

[40] Paul Houston, Dominik Schötzau, and Thomas P. Wihler. ENERGY NORM A POSTERIORI ERROR ESTIMATION OF hp-ADAPTIVE DISCONTINUOUS GALERKIN METHODS FOR ELLIPTIC PROBLEMS. *Mathematical Models and Methods in Applied Sciences*, 17(01):33–62, 2007. doi: 10.1142/S0218202507001826. URL `http://www.worldscientific.com/doi/abs/10.1142/S0218202507001826`.

[41] Birendra Jha and Ruben Juanes. A locally conservative finite element framework for the simulation of coupled flow and reservoir geomechanics. *Acta Geotechnica*, 2(3):139–153, 2007.

[42] Pavel Jiránek, Zdeněk Strakoš, and Martin Vohralík. A Posteriori Error Estimates Including Algebraic Error and Stopping Criteria for Iterative Solvers. *SIAM Journal on Scientific Computing*, 32(3):1567–1590, 2010. doi: 10.1137/08073706X. URL `http://dx.doi.org/10.1137/08073706X`.

[43] J. Kim, H.A. Tchelepi, and R. Juanes. Stability and Convergence of Sequential Methods for Coupled Flow and Geomechanics: Drained and Undrained Splits,. *Computer Methods in Applied Mechanics and Engineering*, 200:2094–2116, November 2011.

[44] Jihoon Kim, H. A. Tchelepi, and R. Juanes. Rigorous Coupling of Geomechanics and Multiphase Flow with Strong Capillarity. *Society of Petroleum Engineers*, 2013. doi: 10.2118/141268-PA.

[45] Xianguo Li and Imran Sabir. Review of bipolar plates in {PEM} fuel cells: Flow-field designs. *International Journal of Hydrogen Energy*, 30(4):359–371, 2005. ISSN 0360-3199. doi: 10.1016/j.ijhydene.2004.09.019. URL `http://www.sciencedirect.com/science/article/pii/S0360319904003453`. Fuel Cells.

[46] Umberto Lucia. Overview on fuel cells. *Renewable and Sustainable Energy Reviews*, 30(C):164–169, 2014. URL `http://ideas.repec.org/a/eee/rensus/v30y2014icp164-169.html`.

[47] Mitchell Luskin, Rolf Rannacher, and Wolfgang Wendland. On the smoothing property of the crank-nicolson scheme. *Applicable Analysis*, 14(2):117–135, 1982. doi: 10.1080/00036818208839415. URL `http://dx.doi.org/10.1080/00036818208839415`.

[48] George Marsh. Fuel cell materials. *Materials Today*, 4(2):20–24, 2001. ISSN 1369-7021. doi: 10.1016/S1369-7021(01)80123-1. URL `http://www.sciencedirect.com/science/article/pii/S1369702101801231`.

[49] D Meidner. *Adaptive space–time finite element methods for optimization problems governed by nonlinear parabolic systems*. PhD thesis, Universität Heidelberg, 2007.

[50] D. Meidner, R. Rannacher, and J. Vihharev. Goal-oriented error control of the iterative solution of finite element equations. *Journal of Numerical Mathematics*, 17:143–172, 2009. doi: 10.1515/JNUM.2009.009.

[51] Dominik Meidner and Boris Vexler. A Priori Error Estimates for Space-Time Finite Element Discretization of Parabolic Optimal Control Problems Part I: Problems Without Control Constraints. *SIAM Journal on Control and Optimization*, 47(3):1150–1177, 2008. doi: 10.1137/070694016. URL `http://dx.doi.org/10.1137/070694016`.

[52] Dominik Meidner and Boris Vexler. A Priori Error Estimates for Space-Time Finite Element Discretization of Parabolic Optimal Control Problems Part II: Problems with Control Constraints. *SIAM Journal on Control and Optimization*, 47(3):1301–1329, 2008. doi: 10.1137/070694028. URL `http://dx.doi.org/10.1137/070694028`.

[53] A. Mikelic and M.F. Wheeler. Convergence of Iterative Coupling for Coupled Flow and Geomechanics. *Computational Geosciences*, 17:455–461, 2013.

[54] S. Mittal, A. Ratner, D. Hastreiter, and T.E. Tezduyar. "Space-Time Finite Element Computation of Incompressible Flows with Emphasis on Flows Involving Oscillating Cylinders. *InternationalVideo Journal of Engineering Research*, pages 83–96, 1991.

[55] P. Möbius. Dautray, R.; Lions, J.-L., Mathematical Analysis and Numerical Methods for Science and Technology. Vol. 3: Spectral Theory and Applications. Berlin etc., Springer-Verlag 1990. X, 515 pp., DM 198,OO. ISBN 3-540-50208-4. *ZAMM - Journal of Applied Mathematics and Mechanics / Zeitschrift für Angewandte Mathematik und Mechanik*, 72(3):237–237, 1992. ISSN 1521-4001. doi: 10.1002/zamm.19920720316. URL `http://dx.doi.org/10.1002/zamm.19920720316`.

[56] Murtazo Nazarov and Johan Hoffman. An adaptive finite element method for inviscid compressible flow. *International Journal for Numerical Methods in Fluids*, 64(10-12):1102–1128, 2010. ISSN 1097-0363. doi: 10.1002/fld.2335. URL `http://dx.doi.org/10.1002/fld.2335`.

[57] Donatien N'dri, André Garon, and André Fortin. Incompressible Navier–Stokes computations with stable and stabilized space–time formulations: a comparative study. *Communications in Numerical Methods in Engineering*, 18(7):495–512, 2002. ISSN 1099-0887. doi: 10.1002/cnm.507. URL `http://dx.doi.org/10.1002/cnm.507`.

[58] Anthony T Patera and EINAR M RØNQUIST. A general output bound result: application to discretization and iteration error estimation and control. *Mathematical Models and Methods in Applied Sciences*, 11(04):685–712, 2001.

[59] Jean H Prevost. Partitioned solution procedure for simultaneous integration of coupled-field problems. *Communications in numerical methods in engineering*, 13(4):239–247, 1997.

[60] R Rannacher and J Vihharev. Adaptive finite element analysis of nonlinear problems: balancing of discretization and iteration errors. *Journal of Numerical Mathematics*, 21(1):23–62, 2013.

[61] Rolf Rannacher. Finite element solution of diffusion problems with irregular data. *Numerische Mathematik*, 43(2):309–327. ISSN 0945-3245. doi: 10.1007/BF01390130. URL `http://dx.doi.org/10.1007/BF01390130`.

[62] Rolf Rannacher, Antje Westenberger, and Winnifried Wollner. Adaptive finite element solution of eigenvalue problems: balancing of discretization and iteration error. *Journal of Numerical Mathematics*, 18(4):303–327, 2010.

[63] CA Ringhofer, C Schmeiser, and Peter A Markowich. *Semiconductor Equations*. Springer, 1990.

[64] M. Schmich and B. Vexler. Adaptivity with Dynamic Meshes for Space-Time Finite Element Discretizations of Parabolic Equations. *SIAM Journal on Scientific Computing*, 30(1):369–393, 2008. doi: 10.1137/060670468. URL `http://epubs.siam.org/doi/abs/10.1137/060670468`.

[65] A. Settari and D. A. Walters. Advances in Coupled Geomechanical and Reservoir Modeling With Applications to Reservoir Compaction. *Society of Petroleum Engineers*, 2001. doi: 10.2118/74142-PA.

[66] Antonin Settari, FM Mourits, et al. A coupled reservoir and geomechanical simulation system. *Spe Journal*, 3(03):219–226, 1998.

[67] Gilbert Strang. VARIATIONAL CRIMES IN THE FINITE ELEMENT METHOD. In A.K. Aziz, editor, *The Mathematical Foundations of the Finite Element Method with Applications to Partial Differential Equations*, pages 689–710. Academic Press, 1972.

[68] Kevin Kendall Subhash C. Singhal. *High-temperature Solid Oxide Fuel Cells*. Elsevier, 2003.

[69] K.E. Swider-Lyons, R.T. Carlin, R.L. Rosenfeld, and R.J. Nowak. Technical issues and opportunities for fuel cell development for autonomous underwater vehicles. In *Autonomous Underwater Vehicles, 2002. Proceedings of the 2002 Workshop on*, pages 61–64, 2002. doi: 10.1109/AUV.2002.1177204.

[70] Vidar Thomée. *Galerkin finite element methods for parabolic problems*, volume 1054. Springer, 1984.

[71] David Tran, Antonin Settari, Long Nghiem, et al. New iterative coupling between a reservoir simulator and a geomechanics module. In *SPE/ISRM Rock Mechanics Conference*. Society of Petroleum Engineers, 2002.

[72] JJW Van der Vegt and H Van der Ven. Space–time discontinuous Galerkin finite element method with dynamic grid motion for inviscid compressible flows: I. General formulation. *Journal of Computational Physics*, 182(2):546–585, 2002.

[73] Rüdiger Verfürth. A posteriori error estimation and adaptive mesh-refinement techniques. *Journal of Computational and Applied Mathematics*, 50(1):67–83, 1994.

[74] Mary F Wheeler and Xiuli Gai. Iteratively coupled mixed and Galerkin finite element methods for poro-elasticity. *Numerical Methods for Partial Differential Equations*, 23(4):785–797, 2007.

[75] Joseph Wloka. *Partial differential equations*. Cambridge [Cambridgeshire] ; New York : Cambridge University Press, 1987. ISBN 0521259142. Translation of: Partielle Differentialgleichungen.

[76] Zhiqiang Zhai and Qingyan (Yan) Chen. Solution characters of iterative coupling between energy simulation and {CFD} programs. *Energy and Buildings*, 35(5):493–505, 2003. ISSN 0378-7788. doi: 10.1016/S0378-7788(02)00156-1. URL `http://www.sciencedirect.com/science/article/pii/S0378778802001561`.